DESIGN AND CHARACTERIZATION OF A SHAPE MEMORY POLYMER FOAM-

COATED COIL NEUROVASCULAR EMBOLIZATION DEVICE

A Dissertation

by

ANTHONY JOHN BOYLE

Submitted to the Office of Graduate and Professional Studies of
Texas A&M University
in partial fulfillment of the requirements for the degree of

DOCTOR OF PHILOSOPHY

Chair of Committee,	Duncan J. Maitland
Committee Members,	John C. Criscione
	Balakrishna Haridas
	Fred Clubb
Head of Department,	Anthony Guiseppi-Elie

December 2016

Major Subject: Biomedical Engineering

ABSTRACT

Standard endovascular treatment of intracranial saccular aneurysms has been shown to be an effective treatment method, but it remains marked by aneurysm recanalization despite continued development of new device technologies. Polyurethane-based shape memory polymer (SMP) foams are advantageous biomaterials for endovascular embolization applications, however previously developed devices utilizing SMP foam for neurovascular embolization treatment were limited by required catheter sizes, insufficient flexibility and radiopacity, and inconsistent device stability within the aneurysm sac.

Solvent-stimulated actuation of hydrophobic SMP foams using DMSO and EtOH was shown to be an effective alternative shape memory trigger to direct heating. Dramatic decreases in T_g were observed with exposure to water, DMSO, and EtOH. Rapid shape recovery and volume swelling were observed for SMP foams in high concentrations of both DMSO and EtOH, as well as in decreased concentrations of EtOH.

A SMP foam-over-wire (FOW) neurovascular embolization device was evaluated using *in vitro* and *in vivo* saccular aneurysm models as an initial prototype design. *In vivo* porcine aneurysms were successfully occluded using FOW devices with theoretical volume occlusion values greater than reported values for predicate devices and rapid, stable thrombus formation. FOW devices were successful in treating sidewall aneurysm models, though the study suggested a need to improve the deliverability and radiopacity of the devices and to evaluate the occlusion effectiveness in more clinically relevant aneurysm geometries.

A SMP foam-coated coil (FCC) embolization device was designed and demonstrated clinician-familiar deliverability and use combined with large packing density and scaffolding capability of porous SMP foam. Excellent cytocompatibility is a promising early result in showing biocompatibility. FCC devices exhibited smooth delivery, but difficult packing in both benchtop and rabbit elastase aneurysm models highlights the need to improving device stiffness. However, though packing in rabbit aneurysms was poor, the tissue response suggests a desired healing process and a promising indication that the more effectively packed FCC devices will prompt stable, long-term tissue healing. Overall, the device designed through this work demonstrates excellent potential for improving long-term clinical outcomes for patients with intracranial saccular aneurysms, whether ruptured or unruptured.

DEDICATION

To my parents, whose unconditional love and selflessness have guided and supported me throughout my life and through the joys and hardships of pursuing my goals.

ACKNOWLEDGEMENTS

NOMENCLATURE

aSAH	Aneurysmal subarachnoid hemorrhage
DI Water	Deionized water
DMA	Dynamic mechanical analysis
DMSO	Dimethyl sulfoxide
DSA	Digital subtraction angiography
DSC	Differential scanning calorimetry
EtOH	Ethyl alcohol
FCC	Foam-coated-coil
FOW	Foam-over-wire
GDC	Guglielmi detachable coil
H&E	Hemotoxylin and eosin
HPED	N,N,N',N'-Tetrakis(2-hydroxypropyl)ethylenediamine
ID	Inner diameter
IPA	Isopropyl alcohol
IPDI	Isophorone diisocyanate
Nitinol	Nickel titanium alloy
OD	Outer diameter
PTAH	Phosphotungstic acid haematoxylin
PDMS	Poly(dimethylsiloxane)
Pt	Platinum
RO Water	Reverse osmosis water

SMP   Shape memory polymer

TEA   Triethanolamine

T_g Glass transition temperature

T_{trans} Transition temperature

W   Tungsten

TABLE OF CONTENTS

LIST OF FIGURES

LIST OF TABLES

CHAPTER I

INTRODUCTION AND LITERATURE REVIEW[*]

1.1 Intracranial Saccular Aneurysms

Aneurysmal subarachnoid hemorrhage (aSAH) occurs when an intracranial aneurysm ruptures causing bleeding into the subarachnoid space in the brain. Intracranial saccular aneurysms occur when the artery wall dilates into a sphere-like sac. As aneurysms develop and grow in size, the aneurysm wall thickness decreases, and stiffness increases, resulting in an increased risk of rupture from constant blood flow and pressure in the aneurysm sac.[1] Saccular aneurysms are typically sized by diameter and range broadly in size from a few millimeters in diameter to tens of millimeters, though they are reported most commonly in the 3-10 mm range.[2] Saccular aneurysms typically develop at the apex of arterial bifurcations in or near the Circle of Willis at the base of the brain and are typically asymptomatic until they rupture, causing aSAH.[3] aSAH incidence occurs in 9.7 – 14.5 out of every 100,000 adults in the United States and is associated with high morbidity and mortality rates. aSAH results in the death of at least 25% of patients, and approximately 50% of survivors are left with persistent neurological deficit.[4] For patients

with a neurological deficit, 30% suffer from permanent damage, and 20% require hospice care for the remainder of their life.[5] Additionally, patients often have more than one aneurysm, increasing the risk of subsequent ruptures.[6] Therefore, prevention of aneurysmal rupture and effective treatment of ruptured aneurysms are essential for reducing morbidity and mortality due to aneurysmal subarachnoid hemorrhage.

1.2 Endovascular Coiling Treatment

Standard endovascular treatment of intracranial saccular aneurysms involves the delivery and implantation of embolization coil devices into the aneurysm with the goal of promoting thrombus formation, tissue healing, and neointima growth across the aneurysm neck.[7] Embolization coils were first introduced to clinical use with the Guglielmi detachable coil (GDC®), a bare platinum coil, in 1990 as an alternative to surgical clipping methods, which require an invasive craniotomy surgical procedure.[8,9] Bare platinum coils are typically constructed of platinum-tungsten (Pt/W) alloy wire wound into a primary coil and are then shaped in either secondary helical, complex, or spherical geometries.[10] During endovascular coiling procedures, a microcatheter is introduced into the femoral artery and navigated to the aneurysm under x-ray fluoroscopy guidance. An embolization coil device is delivered through the microcatheter, deployed into the aneurysm sac, and detached. Multiple coil devices are packed into the aneurysm until the sac is visibly occluded, which can be seen during angiography or digital subtraction angiography (DSA) as shown in Figure 1.1. After implantation, the packed coil mass promotes flow stagnation and thrombus formation, which is an essential early step towards cell infiltration, stable healing, and neointima formation across the aneurysm neck.[7]
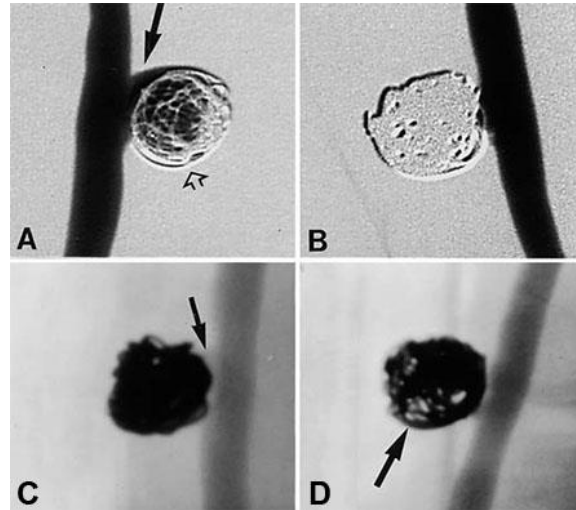
Figure 1.1: Saccular aneurysms post-treatment using GDCs® and bioactive polymer-coated coils. (A) DSA of loosely packed (empty arrow) bioactive polymer-coated coils immediately post-embolization. Contrast is visible at small neck remnant (arrow) and throughout aneurysm. (B) DSA of tightly packed GDCs® immediately post-embolization. (C) Angiography of tightly packed GDCs® immediately post-embolization with small neck remnant (arrow). (D) Angiography of loosely packed (arrow) bioactive polymer-coated coils immediately post-embolization. (Adapted from [11] with permission from JNS Publishing Group)

Endovascular coiling has been shown to be an effective method of treatment for intracranial aneurysms, but it remains limited by aneurysm recanalization or recurrence despite introduction of new technologies.[12,13] In 2005, Molyneux et al. reported that endovascular coiling improved patient independent survival at 1 year compared to neurosurgical clipping.[13] However, endovascular coiling is limited by the risk of aneurysm recurrence or recanalization, which involves the return of blood flow into the occluded aneurysm and increased risk of rupture and hemorrhage. Diminished packing density, defined as the ratio of implanted device volume to aneurysm volume, as well as poor or unstable thrombus organization have been associated with increased recurrence, among

other mechanisms.[14-16] Bare platinum coils have been reported with 30 – 31% packing density and unorganized thrombus formation that may not organize within 3 years following treatment.[17-19] Early studies of recurrence rates following treatment using bare platinum coils reported recurrence in 21 – 34% of cases.[20,21] Based on these limitations, polymer-embedded coils were introduced to improve healing and reduce recanalization rates. Biodegradable polymers were used in coil devices, such as Matrix® and Cerecyte®, in order to accelerate the inflammation response as a means of stimulating mature tissue healing not found with bioinert bare platinum coils.[19,22] However, Matrix® coils resulted in worse recurrence rates in early studies and no significant difference in recurrence in later randomized clinical study compared to bare platinum coils.[23-25] Furthermore, Cerecyte® coils have resulted in no significant difference in angiographic outcomes compared to bare platinum coils in randomized clinical trials.[26] HydroCoil® devices were also introduced to improve recurrence rates by means of increasing packing density.[27] HydroCoils® are coils coated with a hydrogel that expands over time during contact with water, displacing blood and filling the majority of the aneurysm space.[17] However, although they have increased packing densities compared to other coil devices, HydroCoils® have not resulted in significantly improved long-term clinical outcomes.[28] Overall, new coil technologies have not improved recurrence rates, and clinical recurrence remains a primary limitation of endovascular coiling, occurring in 21% of cases and requiring retreatment in 10% of cases.[12]

4

1.3 Shape Memory Polymer Foams

Shape memory polymers (SMP) are a unique class of materials capable of maintaining a programmed shape and subsequently recovering their original shape in response to a stimulus such as heat, light, or moisture.[29,30] Thermo-responsive SMPs act about a transition temperature (T_{trans}) during the shape memory cycle. The SMP is heated above T_{trans}, deformed into its programmed state into an increased stress configuration, and cooled below T_{trans}, where low polymer chain mobility holds the SMP in its programmed shape. To actuate the polymer and induce shape recovery, the SMP is heated above T_{trans}, and high polymer chain mobility allows entropic forces in the polymer chains to recover to the decreased stress configuration of the original shape of the SMP. Shape recovery percentage, defined as the percentage ratio of the recovered strain to the original strain, is a key metric of the shape memory cycle and used to evaluate the effectiveness of shape recovery. Figure 1.2 illustrates the shape memory cycle for a thermo-responsive SMP.
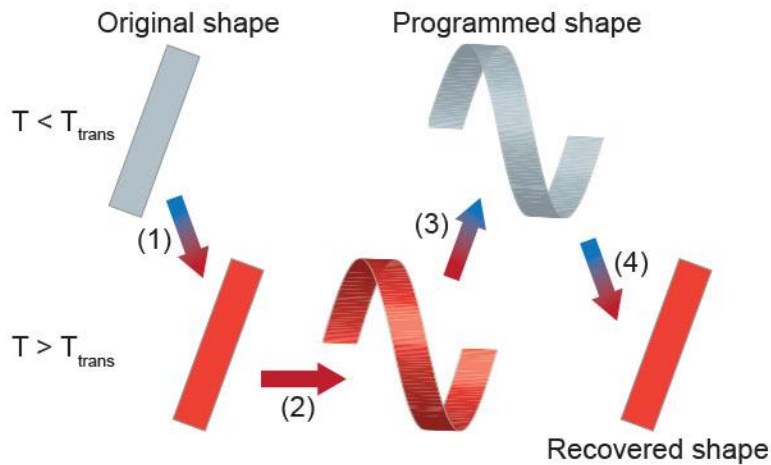
Figure 1.2: The shape memory cycle for a thermo-responsive shape memory polymer. (1) Heating above T$_{trans}$. (2) Deforming to programmed geometry while T > T$_{trans}$. (3) Cooling below T$_{trans}$ while holding programmed shape. (4) Heating above T$_{trans}$ to recover original shape.

Polyurethane-based SMP foams have been proposed as an advantageous biomaterial for endovascular embolization applications due to their shape recovery capability and interconnected, large surface area porosity.[1,31,32] Wilson et al. synthesized highly crosslinked, amorphous polyurethane SMPs from uniform, aliphatic monomers for use in medical devices.[29] For endovascular embolization applications, the SMPs were fabricated into a porous foam structure in order to achieve large volume recovery and high surface area properties.[33] These porous SMPs have been reported with tunable physical, mechanical, and chemical properties, including but not limited to low bulk densities near 0.015 g/cm^3, sharp glass transition temperatures (T$_g$) ranging 45 – 75 °C, and consistent shape recovery greater than 80%.[33,34] Figure 1.3 shows the interconnected porosity of the SMP foams. SMP foam composites have also been fabricated using additives such as

tungsten and barium sulfate in order to provide x-ray radiopacity and/or tune mechanical properties.[35-37] Furthermore, biocompatibility of the polyurethane-based SMP foams has been evaluated via preliminary benchtop models and porcine animal models. SMP foams have been reported with promising cytocompatibility, increased implanted angiographic occlusion, integrated connective tissue post-implant, and thicker neointima layer compared to bare platinum coils in porcine saccular aneurysm models.[1,31,33] The interconnected porosity of the SMP foams acts as a scaffold for blood flow and thrombus formation throughout the material volume. This morphology contrasts with hydrogel materials used in endovascular coils that have pore sizes less than 10 µm and displace blood out of the aneurysm volume.[1,31] The material properties and characteristics of these polyurethane-based SMP foams lend them to a novel volume filling and tissue scaffolding solution to endovascular embolization procedures.
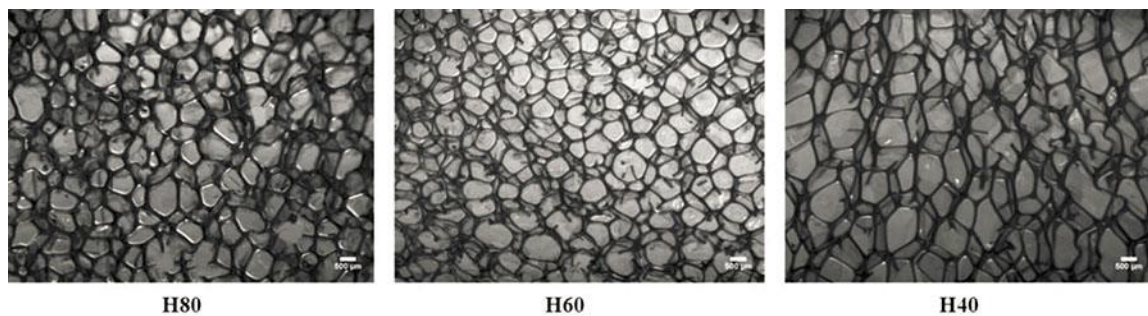
Figure 1.3: Representative cell structure of foams for all the formulations H80 through H40. Foams of all formulations show a mixed, closed to open cell structure, with thin cell membranes between struts. All scale bars are 500 µm. (Adapted from [33] with permission from John Wiley and Sons)

7

1.4 Rationale for Using Organic Solvents for SMP Actuation

Solvent exposure has been investigated to trigger SMP actuation as an alternative to direct heating or stimulation by electricity, light, or magnetic fields.[38-40] Solvent exposure promotes SMP actuation by swelling into the polymer and plasticizing the polymer chains, thereby increasing chain mobility and lowering T_{trans} below the environment temperature. Figure 1.4 illustrates the use of solvent to stimulate SMP actuation by change in T_{trans}. Solvent-stimulated actuation avoids limitations of direct heating actuation in endovascular applications including poor energy delivery to devices due to heat convention of blood flow and risk of heat-induced tissue damage. However, previous studies have focused on water as the actuating solvent, which is disadvantageous for endovascular applications as devices are exposed to water throughout the entire procedure. Polyurethane-based SMP foams have been reported as water-responsive materials, exhibiting depressed T_g when exposed to water, which actuates and expands compressed devices in physiological conditions.[41,42] For water-responsive embolization materials such as the hydrogel used in HydroCoil® devices and SMP foam implants, endovascular delivery and device repositioning can be significantly impeded or halted due to device swelling or expansion. Singhal et al. reported that increasing hydrophobicity of polyurethane-based SMP foams resulted in delayed self-actuation due to T_g depression in water.[41] Although water stimulated actuation design of SMPs provides simpler clinical procedures and reduced risk of tissue damage due to a heating device for actuation, the procedure is dependent on inconsistent actuation timing. Sufficient working time, the time in which the device can be repositioned and retracted back into the microcatheter prior to

self-actuation, through SMP foam hydrophobicity has yet to be achieved without severely extending the time for self-actuation or completely preventing it at physiological conditions. Solvent actuation of SMP materials using organic solvents can provide clinician-initiated and controlled actuation without direct heating. Organic solvent–actuated SMP foams that exhibit significantly delayed or no self-actuation in water provide long working times for clinicians while retaining expansion capabilities for improved aneurysm filling over platinum coils.
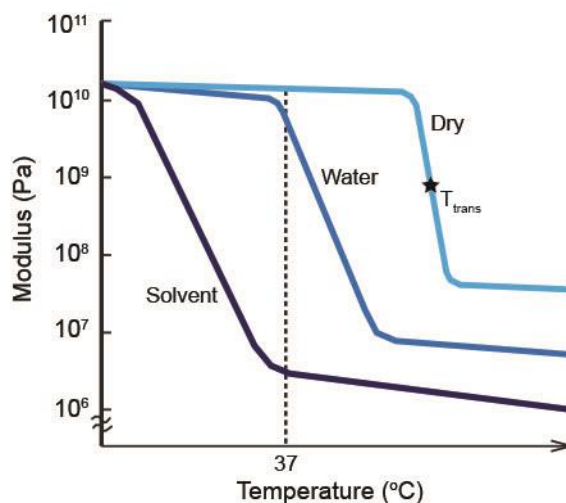
Figure 1.4: Example of SMP transition temperature (T_{trans}) change in response to contact with water or other solvents.

However, the injection of organic solvents during endovascular procedures can result in pharmacological and toxicological effects on the tissues. Dimethyl sulfoxide (DMSO) has been used as a solvent in commercially available liquid embolic materials for treatment of intracranial aneurysms and arteriovenous malformations.[43-45] Onyx® is a

9

liquid embolic treatment for intracranial aneurysms that implements a polymer dissolved in DMSO at 92 – 94% by volume that is carefully injected and subsequently allowed to precipitate out of the DMSO solution by blood flow. Onyx® has been successfully used clinically since its introduction, motivating interest in DMSO as a solvent for neurovascular applications, though research into the toxicological effects of DMSO has raised concerns. Liquid intra-arterial infusion of anhydrous DMSO has resulted in full-thickness angionecrosis and severe vasospasm.[46,47] However, low dose volumes of 0.5 – 0.8 mL with slow dose durations over 30 – 120 seconds have been shown to result in significantly less angiotoxicity.[48,49] In addition, the LD_{50} for lysis of red blood cells as total volume percent in whole blood has been reported for DMSO as 5.1%. In comparison, the use of ethanol resulted in a LD_{50} for red blood cell lysis of 21.2%.[50] Ethanol has also been previously studied for liquid embolic applications and use as a parenteral solvent with injections at concentrations ranging 10 – 100% depending on application.[46,47,51] Intra-arterial infusions using ethanol at high concentrations of 70% have produced histological changes and full-thickness angionecrosis while infusions with concentrations of 10 – 40% resulted in necrosis of only the intimal and partially of the medial layer.[46,47] Though different solvents will result in varying degrees of angiotoxicity, studies with both DMSO and ethanol indicated that decreasing the injected solvent concentration resulted in reduced toxicity. Therefore, characterizing the SMP foam expansion at varying solvent concentrations is imperative to determining the clinical feasibility of solvent actuation.

The feasibility of using organic solvent–stimulated actuation of SMP foams has yet to be fully understood, either in general or for endovascular applications. Therefore, this

10

research aimed to investigate if rapid SMP actuation can be achieved and the necessary concentration of solvent in water for clinically relevant expansion times using current hydrophobic SMP foams. Solvent-stimulated actuation is a potentially useful alternative for actuation of a SMP-based endovascular embolization device in intracranial aneurysm treatment, though the method is applicable to several SMP systems for many uses, including non-biomedical. Thus, the work discussed here focuses on developing and characterizing solvent actuation of SMP foams as a foundation for broad clinical application, not only for intracranial aneurysm treatment.

1.5 Rationale for a SMP Foam-Coated Coil Device Design

A new endovascular embolization device must address design constraints of the complex geometry and physiologic environment of the cerebral vasculature while also implementing design inputs proposed to improve clinical outcomes over current commercial devices. During the clinical procedure, the device must be deliverable through a tortuous pathway with minimal resistance, be able to be retracted back into the microcatheter and repositioned multiple times prior to detachment, and be packed into aneurysm volume without entering the parent artery. The device must also exhibit biocompatibility and be clearly visualized with fluoroscopy. Additionally, a new device should provide some approach to improve aneurysm recurrence rates compared to previous devices as a means of improving overall clinical outcomes. A device capable of increasing aneurysm packing density compared to bare platinum coils and promoting mature thrombus organization is hypothesized to decrease recurrence rates and improve long-term clinical outcomes.[14-16]

11
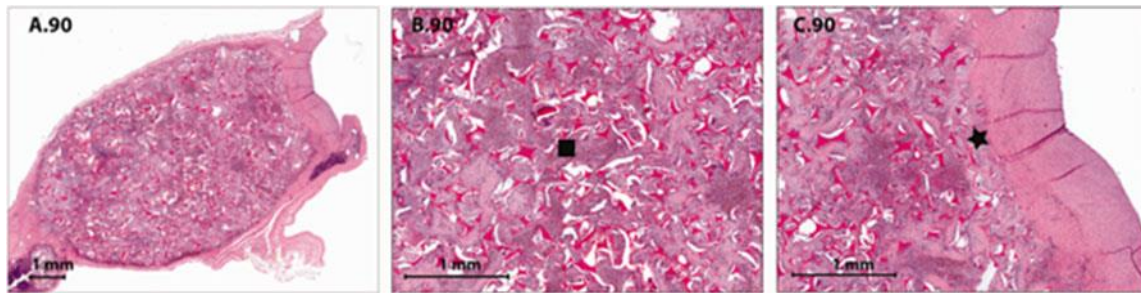
Figure 1.5: H&E Staining (1× and 4× magnification): (A.90) 1× H&E staining of a bisected aneurysm after 90 days of implantation, (B.90) 4× H&E staining of the central core (square) of the bisected aneurysm after 90 days of implantation, and (C.90) 4× H&E staining of foam and parent artery interface (star) after 90 days of implantation. All scale bars are 1 mm. (Adapted from [1] with permission from John Wiley & Sons)

A shape memory polymer (SMP) foam-coated coil embolization device can provide the volume filling and large surface area properties of SMP foams combined with the fluoroscopic contrast and mechanical stability of bare platinum coils. The low densities and excellent shape recovery capabilities of SMP foams enable both delivery of a compact device through a microcatheter and subsequent expansion to increase bulk volume filling per device length compared to current commercial devices.[33,34] Furthermore, polyurethane-based SMP foams can be actuated using exposure water, blood, or saline, and the expansion kinetics can be tuned to allow for sufficient working time and can achieve effective volume filling.[34,41] Though both SMP foams and hydrogels in HydroCoils® exhibit volume filling capability, SMP foams exhibit interconnected pores with diameters in the hundreds of microns compared to hydrogel pore sizes, which are less than 10 µm.[33,52] Therefore, compared to HydroCoils®, which displace blood and thrombus from the aneurysm volume,

12

the interconnected porosity of the SMP foams has been shown to act as a scaffold for blood flow, thrombus formation, and connective tissue healing throughout the material volume in porcine saccular aneurysm models.[1,31] Thus, the SMP foam occlusion is achieved primarily with thrombus and tissue supported with a small volume of foam scaffold. Figure 1.5 shows the 90-day histology of the polyurethane-based SMP foam implanted in a porcine saccular aneurysm model. SMP foams implanted in porcine saccular aneurysm models also resulted in complete endothelialization across the aneurysm ostium with minimal inflammation.[1,31] However, clinical applications of previously studied devices comprised solely of SMP foam are limited due to the need for catheter sizes that are incompatible with the cerebral vasculature, insufficient flexibility through tortuous neurovascular anatomy, insufficient radiopacity for fluoroscopic imaging, and inconsistent device stability in the aneurysm, resulting in SMP foam migration into the parent artery.[32] These limitations can be addressed by combining the novel characteristics of SMP foams with a compliant, radiopaque backbone. Platinum-tungsten alloy coils are standard materials in endovascular embolization coil devices and are capable of providing both excellent compliance and x-ray radiopacity.[10] Furthermore, secondary shaping of embolization coils has been shown to improve control of deployment and aneurysm packing. Nickel-titanium (nitinol) alloys have previously been used as superelastic materials for biomedical applications, including neurovascular, and are hypothesized to be an effective material for shaping the SMP foam-coated coil into secondary geometries.[53,54] Overall, the SMP foam-coated coil embolization device is hypothesized to improve

13

aneurysm volume occlusion and tissue healing with deliverability and use that is familiar

to clinicians, resulting in an effective device with a low adoption hurdle for clinicians.

CHAPTER II

SOLVENT STIMULATED ACTUATION OF POLYURETHANE-BASED SHAPE

MEMORY POLYMER FOAMS USING DIMETHYL SULFOXIDE AND ETHANOL[*]

2.1 Introduction

Shape memory polymers (SMPs) are promising materials due to their ability to maintain a temporary shape and subsequently recover their original shape in response to a thermal, chemical, or optical stimulus.[29,30,55] Thermoresponsive SMPs act about a transition temperature (T_{trans}), where below T_{trans}, low polymer chain mobility holds the SMP in its temporary shape and above T_{trans}, high polymer chain mobility allows entropic forces in the polymer chains to recover the original shape of the SMP. Porous SMPs exhibit volume expansion, high surface area-to-volume ratios, permeability, and thermomechanical properties that are advantageous for several applications including biomedical, aerospace, self-healing materials, and textiles.[1,29,33]

Solvent exposure has been investigated to trigger SMP actuation as an alternative to direct heating or stimulation by electricity, light, or magnetic fields.[38-40] Solvent exposure promotes SMP actuation by plasticizing the polymer chains, thereby increasing chain mobility and lowering T_{trans} below the environment temperature. Previous studies have focused on water as the actuating solvent, which is not ideal for several applications where water exposure is common to the environment.[38,39,56] With water-responsive SMPs,

water exposure can result in decreased stiffness and stimulate actuation prior to successful placement of the material, reducing the effectiveness of porous SMPs for applications such as water filtration, textiles, and clinical embolic vascular devices. Porous polyurethane SMP foams have been reported as water-responsive materials.[41,42] Singhal et al. reported that increasing SMP foam hydrophobicity resulted in delayed actuation in aqueous environments, but the actuated volume was severely reduced.[41] Actuation of non-water-responsive SMPs with an alternative solvent can provide controlled SMP expansion without direct heating and minimize the negative effects of water plasticization on material performance and mechanical properties.

This study aims to investigate the feasibility and sensitivity of solvent-stimulated SMP foam actuation with an initial focus of aqueous environments of biomedical applications. Two organic solvents were chosen due to an expectation of effective polyurethane plasticization and their previous use in biomedical applications: dimethyl sulfoxide (DMSO) and ethanol (EtOH). DMSO has been used as a solvent in transdermal drug delivery and liquid embolic materials.[43,57] EtOH has also been studied for liquid embolic applications and for use as a parenteral solvent.[46,47,51] However, both DMSO and EtOH have been shown to have concentration dependent toxicological effects, indicating a need for using diluted solvent solutions for biomedical applications.[46,47] SMP foam compositions with varying hydrophobicity were investigated for changes in thermo-mechanical properties and shape recovery when exposed to water and varying concentrations of organic solvents.

2.2 Materials and Methods

2.2.1 Shape Memory Polymer Foam Fabrication

Polyurethane-based shape memory polymer (SMP) foams were synthesized using a two-step method with aliphatic isocyanate and hydroxyl monomers as previously reported.[41] Trimethyl-1,6-hexamethylene diisocyanate, 2,2,4- and 2,4,4- mixture (TMHDI, TCI America Inc.), isophorone diisocyanate (IPDI, 98%; Sigma-Aldrich Inc.), N,N,N',N'-tetrakis(2-hydroxypropyl)ethylenediamine (HPED, 99%; Sigma-Aldrich Inc.), triethanolamine (TEA, 98%; Sigma-Aldrich Inc.), DC 198 (Air Products and Chemicals, Inc.), DC 5943 (Air Products and Chemicals, Inc.), T-131 (Air Products and Chemicals, Inc.), BL-22 (Air Products and Chemicals, Inc), Enovate 245fa Blowing Agent (Honeywell International, Inc.) and deionized (DI) water (> 17 M Ω cm purity; Millipore water purifier system; Millipore Inc.) were used as received. SMP foam compositions were synthesized with 0, 10, and 20 mol% of IPDI, with the remaining isocyanate mol% comprised of TMHDI, as previously reported by Hasan et al.[34] The SMP foam compositions are denoted by the respective mol% of IPDI as 0IPDI, 10IPDI, and 20IPDI.

After the synthesis, SMP foams were processed before being cut into blocks for reticulation. As reported by Rodriguez et al, a mechanical wire punch apparatus was used for reticulation.[58] 8 mm diameter, 2-3 cm long cylindrical samples were cut from the foam blocks using a biopsy punch. The foam samples were radially compressed to 1 mm diameter using a SC250 stent crimper (Machine Solutions, Inc., Flagstaff, AZ), heated to 100 °C, and subsequently heated to expand to their original shape. SMP foam cylinders

17

were then acid etched, cleaned under sonication, and dried under vacuum, as previously reported.[34] Foam samples were stored in a sealed container with desiccant.

2.2.2 SMP Foam Density and Pore Diameter

SMP foam density was measured for each composition. Bulk foams were cut into cubes using a resistive wire cutter from three sections along the foaming axis in accordance with ASTM standard D-3574. The length of each cube edge was measured using calipers to calculate volume, mass was measured for each foam cube, and density was calculated.

Pore diameter was measured for each SMP foam composition. Each pore is approximately uniform in diameter in the transverse direction and elongated in the axial foaming direction. Cleaned SMP foam cylinders were cut into 2-3 mm thick slices along the axial and transverse directions. The samples were mounted on a stage and sputter coated with gold for 60 seconds at 20 mA using a Cressington Sputter Coater (Ted Pella, Inc., Redding, CA). Images were taken using a Joel NeoScope JCM-5000 Scanning Electron Microscope (SEM) (Nikon Instruments, Inc., Melville, NY) at 10 kV and 24x magnification under high vacuum. ImageJ software (National Institutes of Health, Bethesda, MD) was used to measure the maximum diameter of seven pores per sample in the axial and transverse directions for two samples of each foam composition.

2.2.3 Differential Scanning Calorimetry

Differential scanning calorimetry (DSC) using a Q-200 DSC (TA Instruments, Inc., New Castle, DE) was used to measure the glass transition temperature (T_g) for approximately 9 mg +/- 3.0 mg of dry and solvent-swelled samples. The dry sample heating profile was ambient to -40.0 °C, isothermal for 2 min, ramp to 120 °C, isothermal for 2

min and repeat. The second heating cycle was used to find the half height transition (T_g) using TA instrument analysis software.

Solvent-swelled samples were first submerged in the selected solvent at 37 °C for 10 min before being mechanically compressed for 2 min to remove residual solvent. The samples were then sealed in TZero pans and placed in the DSC. Samples were cooled to -40 °C from ambient temp, followed by heating to 80 °C (DMSO and Water) or 60 °C (EtOH), isothermal for 2 min, cooled back to -40 °C, and then reheated to the same peak temperature. For all testing, the heating rate was 10 °C/min. A sample size of 3 was used for analysis.

2.2.4 Dynamic Mechanical Analysis

Dynamic mechanical analysis (DMA) was performed to determine the mechano-thermal transitions in various solvents. A TT-DMA (Mettler-Toledo AG, Schwerzenbach, Switzerland) was used to perform kinetic and temperature sweeps, applying a static force of 0.04 N at a rate of 1 Hz, with a static to dynamic force ratio of 1.5. Foam cylinders (6 mm diameter and 5 mm length) were heated to 100 °C and axially compressed to 0.8 mm before cooling to room temperature under compression.

Temperature sweeps were used to find the storage modulus (E') and loss modulus (E'') with the T_g measured as the temperature of the peak ratio of E'/E'' (tan δ). Solvent was cooled to 5 °C or the freezing point of the solvents before being ramped to approximately 70 °C at a rate of 1 °C/min. E' was normalized for each sample to the first measurement and plotted vs time. T_g values for each composition were compared to dry T_g

19

values at tan δ reported by Hasan et al.[34] Four samples were examined for each composition for each solvent.

Kinetic experiments were used to analyze the actuation of SMP foams submerged in solvent over time. Solvent was isothermal at 37 °C for 20 minutes before the sample was submerged, and measurements were recorded for 30 min. E' was normalized for each sample to the first measurement and plotted vs time. The n-values for each foam composition in water, DMSO, and EtOH were three, seven, and four, respectively, to account for variability in kinetic behavior. Kinetic experiments were correlated with temperature sweeps to ensure measurement accuracy.

2.2.5 Swelling Ratio in Solvent Solutions

Swelling volume ratio was measured over time for each SMP foam composition in solvents. SMP foam discs (6 mm diameter and 4-5 mm length) were cut from cleaned and dried samples. A 0.09 mm diameter nickel-titanium (nitinol) wire (Nitinol Devices & Components, Inc., Fremont, CA) was placed through the disc axis. Sample were then imaged, and the sample diameter and length were measured using ImageJ software.

SMP foam samples were submerged in solvent solutions held at 37 ± 1 °C and imaged at fixed time intervals. An aluminum fixture was used to suspend the foam samples in the solution and act as a reference scale. Samples were submerged in solution and were imaged at 1 min intervals for 5 min of submersion and then at 5 min intervals to 15 min total submersion time. ImageJ software was used to measure the diameter and length of samples at each time point. Volume was calculated for the samples at each time point. Volume ratio % at each time point was calculated using (2.1). Volume ratio of 100%

represents the initial volume, while 150% and 200% volume ratio indicate radial swelling of 1.14x and 1.26x, respectively. Swelling volume ratio was measured for 3 samples of each SMP foam composition in water, DMSO, and EtOH.

$$Volume\ Ratio\ \% = \left(\frac{Volume_{Submersion\ Time\ Point}}{Volume_{Initial}}\right) \times 100 \qquad (2.1)$$

2.2.6 Shape Recovery in Solvent Solutions

Shape recovery was measured over time for each SMP foam composition in solvent solutions with varied concentrations. SMP foam cylinders (2.5 mm diameter and 1 cm length) were cut from cleaned and dried samples using a biopsy punch. A 0.09 mm diameter nitinol wire was placed through the cylinder axis. The sample diameter and length were measured for each SMP foam sample using calipers to calculate pre-compressed volume. The SMP foam cylinders were radially compressed to 0.30-0.34 mm diameter using a SC250 stent crimper heated to 100 °C. Compressed samples were stored in a sealed container with desiccant for minimum of 24 hours before testing.

SMP foam samples were submerged in solvent solutions held at 37 ± 1 °C and imaged at fixed time intervals. An aluminum fixture was used to suspend the foam samples in the solution and act as a reference scale. Samples were submerged in solution and were imaged at 1 min intervals for 10 min of submersion and then at 5 min intervals to 30 min total submersion time. ImageJ software was used to measure the diameter and length of actuated sections at each time point. Actuated volume was calculated for the cylindrical samples at each time point. Volume recovery at each time point was calculated using (2.1) where volume ratio of 100% represents the initial volume. Volume recovery was measured for 3 samples of each SMP foam composition in water, DMSO, and EtOH solutions. SMP

foam samples were tested in DMSO concentrations of 100, 90, 80, 40, and 0 vol% in water and in EtOH concentrations of 100, 80, 50, 20, and 0 vol% in reverse osmosis (RO) water, where 0 vol% is the control in 100% RO water.

2.3 Results and Discussion

2.3.1 SMP Foam Morphology

SMP foams were fabricated with similar stable morphology, as shown in Figure 2.1. Cell membranes are still present with small pinholes created during the reticulation process, resulting in a high total surface area with interconnected pores that allow fluid flow through the foam volume.[58] SMP foams were fabricated with varying isocyanate ratios and similar average densities and average pore sizes, as shown in Table 2.1. All SMP foam compositions exhibited transverse anisotropy, where pore diameter is greater in the axial direction than in the transverse direction.
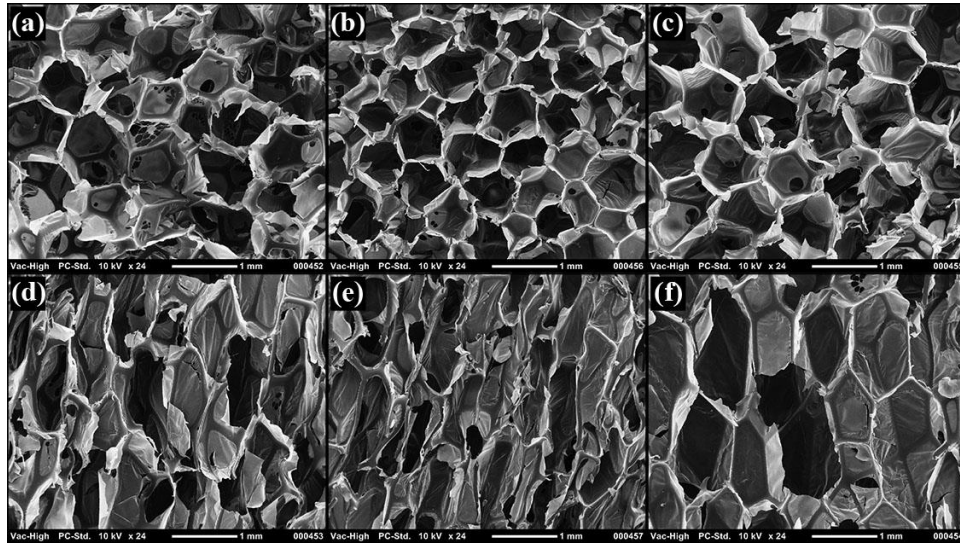
Figure 2.1: SEM images of SMP foams. Foam pores in the transverse direction are shown on the top row for (a) 0IPDI, (b) 10IPDI, and (c) 20IPDI compositions. Foam pores in the axial direction are shown on the bottom row for (d) 0IPDI, (e) 10IPDI, and (f) 20IPDI compositions.

Table 2.1: SMP foam density and pore diameter (mean ± standard deviation)

Foam ID	Density (g/cm^3) (n=2)	Transverse Pore Diameter (μm) (n=14)	Axial Pore Diameter (μm) (n=14)
0IPDI	0.0138 ± 0.0009	680 ± 130	1070 ± 300
10IPDI	0.0111 ± 0.0003	600 ± 150	1070 ± 220
20IPDI	0.0121 ± 0.0002	660 ± 130	1090 ± 210

2.3.2 Glass Transition Temperature Shift

SMP foam glass transition temperatures varied in response to exposure to different solvents with greatest decreases in T_g after exposure to EtOH. Average T_g values for each SMP foam composition measured using DSC and DMA in the dry condition and after submersion in water, DMSO, and EtOH are shown in Table 2. 20IPDI was the only composition to exhibit a water-submerged T_g above body temperature (37 °C), indicating minimal actuation at body temperature. Increasing IPDI content resulted in an increase in T_g in all cases when measured by DMA, due to decreased bond rotation. However, 10IPDI foams demonstrated lower T_g than both 0IPDI and 20IPDI foams with solvent exposure when measured by DSC. This suggests increased plasticization of 10IPDI foams, particularly in DMSO, though there is insufficient data to conclude any statistical significance. From these results, it's suggested that increasing IPDI content is effective at muting or preventing SMP actuation in water while allowing for actuation in DMSO and EtOH.

Table 2.2: Summary of actuation transitions of SMP foams in solvent (mean ± standard deviation)

Foam ID	Dry		Water		DMSO		EtOH	
	T_g (DSC) (°C) (n=3)	T_g (tan δ_{max}) (°C) [34]	T_g (DSC) (°C) (n=3)	T_g (tan δ_{max}) (°C) (n=3)	T_g (DSC) (°C) (n=3)	T_g (tan δ_{max}) (°C) (n=7)	T_g (DSC) (°C) (n=3)	T_g (tan δ_{max}) (°C) (n=4)
0IPDI	66 ± 1	105 ± 2	35 ± 2	46 ± 1	8 ± 3	28 ± 6	-6 ± 4	18 ± 1
10IPDI	74 ± 1	118 ± 2	33 ± 1	51 ± 1	-1 ± 3	33 ± 1	-9 ± 5	18 ± 3
20IPDI	79 ± 2	131 ± 1	44 ± 4	61 ± 1	12 ± 3	41 ± 3	2 ± 4	22 ± 8

2.3.3 Actuation Kinetics and Profiles

Kinetic experiments exhibited distinct actuation transitions in the relaxation behavior of the SMP foams submerged in DMSO and EtOH at 37 °C. Relaxation times were longest in water and shortest in EtOH as shown in Figure 2.2, where the normalized storage modulus is shown for 20IPDI in each solvent. For water and DMSO, no relaxation behavior was seen within 30 minutes, as demonstrated by the lack of a decreasing inflection in the in normalized modulus. However, DMSO does begin to show reduction in modulus within the examined time, contrasted to the modulus increase exhibited in water. In contrast, SMP foams in EtOH demonstrated rapid relaxation within 1 minute. The increased rate of actuation for all foams in EtOH compared to in DMSO is supported by Table 1, where average T_g values are 8 – 19 °C less in EtOH compared to DMSO values. Figure 2.3 illustrates the actuation behavior of all foam compositions submerged in EtOH. 0IPDI and 10IPDI foams actuated at a slightly increased rate in EtOH compared to 20IPDI, though high variance was observed and relaxation time differed by less than 1 minute.
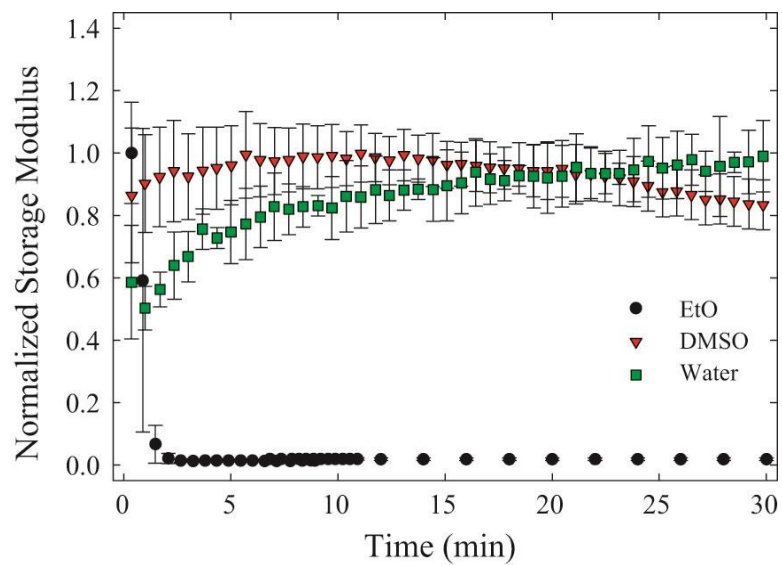
Figure 2.2: Actuation of 20IPDI foam immersed in varying solvents at 37 °C, demonstrated with measurements of storage modulus over time normalized to the initial modulus value.
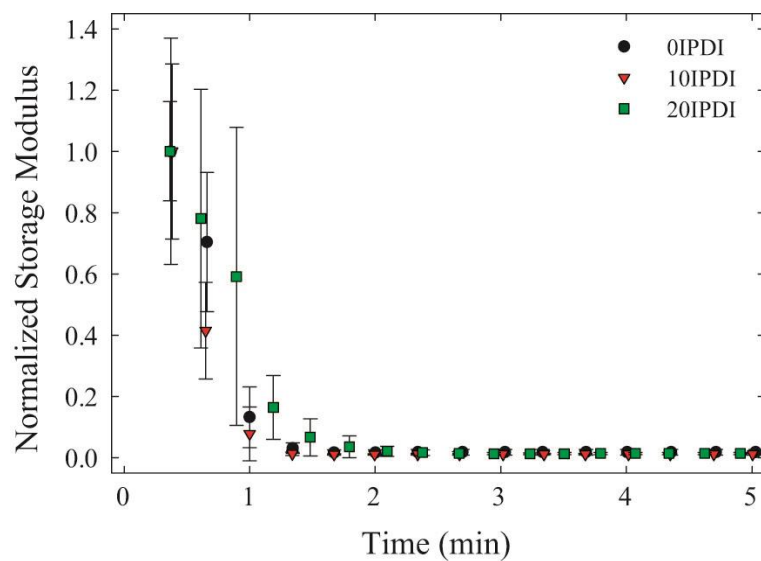
Figure 2.3: Actuation of varying SMP foam compositions immersed in 37 °C EtOH, demonstrated with measurements of storage modulus over time normalized to the initial modulus value.

Swelling tests showed significant increase in SMP foam volume after submersion in DMSO and EtOH and minimal to no volume increase in water. All SMP foam compositions exhibited noticeable swelling within 5 min of exposure to DMSO and within 2 min of exposure to EtOH as shown in Figure 2.4. Volume ratio of 100% represents the initial volume, while greater than 100% volume recovery represents solvent swelling into the polymer, where 150% and 200% volume recovery indicate radial swelling of 1.14x and 1.26x, respectively. 10IPDI foam experienced swelling to greater than 175% volume in both solvents. However, decreased IPDI resulted in greater swelling in DMSO while increased IPDI resulted in greater swelling in EtOH. SMP foams experienced less swelling in water, exhibiting volume ratio % values of 104 ± 1.7% for 0IPDI, 109 ± 8.3% for 10IPDI, and 108 ± 1.4% for 20IPDI after 15 min exposed to water.
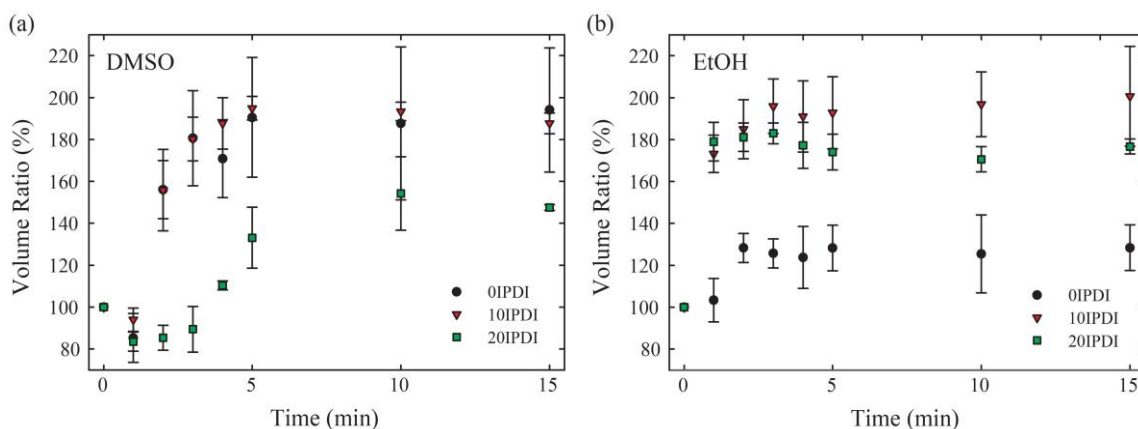
Figure 2.4: Swelling volume ratio in 37 °C solvent solutions. Volume ratio is shown over time of submersion in (a) DMSO and (b) EtOH.

Volume recovery testing demonstrated that submersion in water resulted in minimal foam actuation for all compositions while DMSO and EtOH both stimulated actuation with a solvent concentration dependence, as shown in Figures 2.5 and 2.6. Figure 2.7 shows selected images of the foam actuation in 100% and 20% EtOH solutions. All SMP foam compositions actuated to less than 15% volume recovery in water after 30 min, with 20IPDI actuating the least amongst compositions to less than 3% volume recovery. All SMP foam compositions exhibited greater than 100% volume recovery in 100% and 90% DMSO solutions after 20 min submersion. However, minimal actuation was observed in DMSO concentrations less than 90%, with only 10IPDI in 80% DMSO actuating greater than 30% volume recovery. All SMP foam compositions exhibited greater than 100% volume recovery in 100% and 80% EtOH solutions after 3 min submersion. 0IPDI and 20IPDI actuated to greater than 100% volume recovery in 50% EtOH within 3 min, and 0IPDI and 10IPDI actuated to greater than 100% volume recovery in 20% EtOH within 25 min. Volume recovery testing demonstrates a plasticization sensitivity to EtOH that is not shown with DMSO, where the EtOH is sufficiently more effective as a plasticizer over water, even in dilute concentrations.
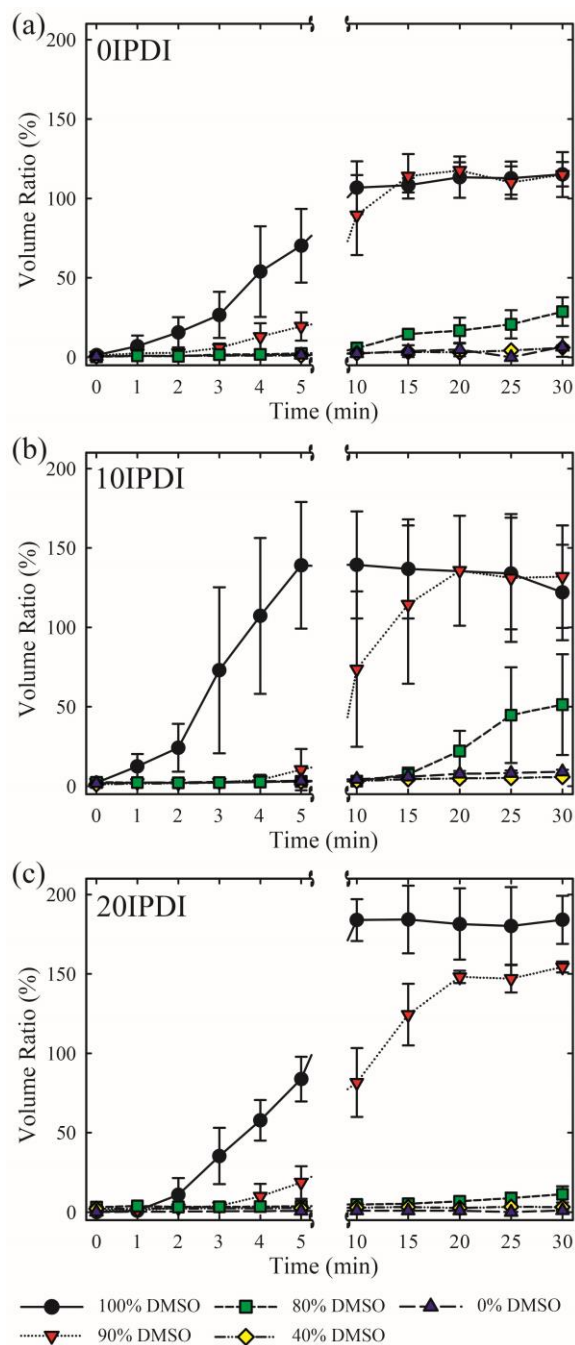
Figure 2.5: Volume recovery in 37 °C DMSO solutions. Volume recovery is shown over time of submersion in DMSO solutions of varying concentrations for SMP foam compositions of (a) 0IPDI, (b) 10IPDI, and (c) 20IPDI, where 0% DMSO is 100% RO water. Note the break in the Time axis between 5 and 10 min.
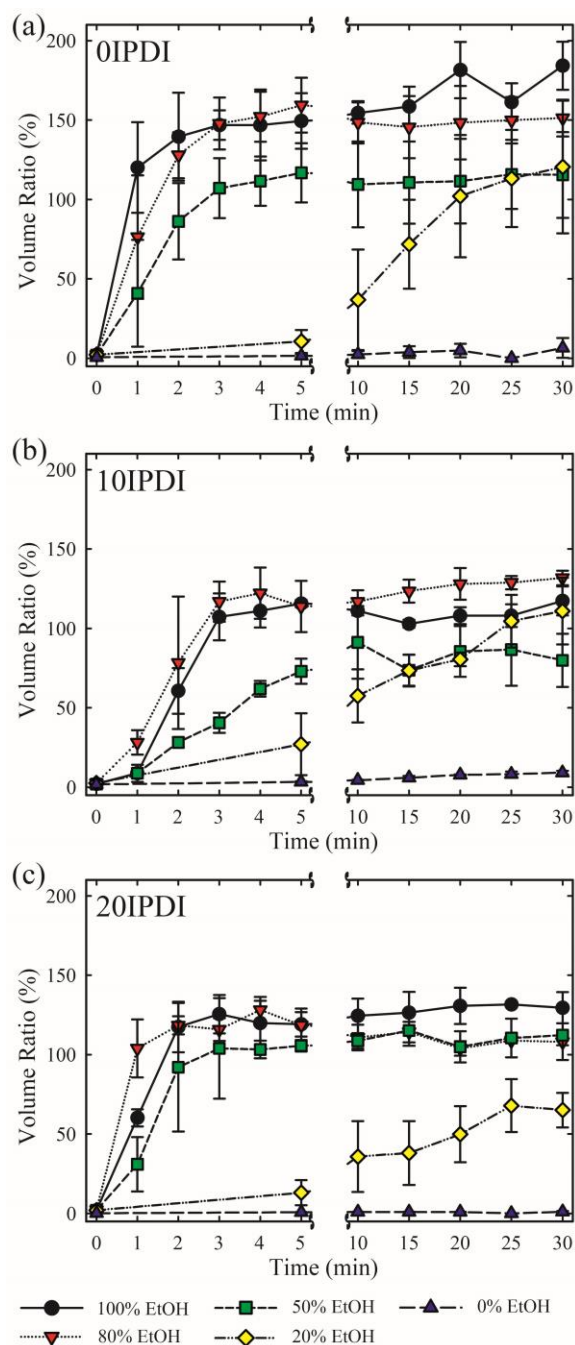
Figure 2.6: Volume recovery in 37 °C EtOH solutions. Volume recovery is shown over time of submersion in EtOH solutions of varying concentrations for SMP foam compositions of (a) 0IPDI, (b) 10IPDI, and (c) 20IPDI, where 0% EtOH is 100% RO water. Note the break in the Time axis between 5 and 10 min.
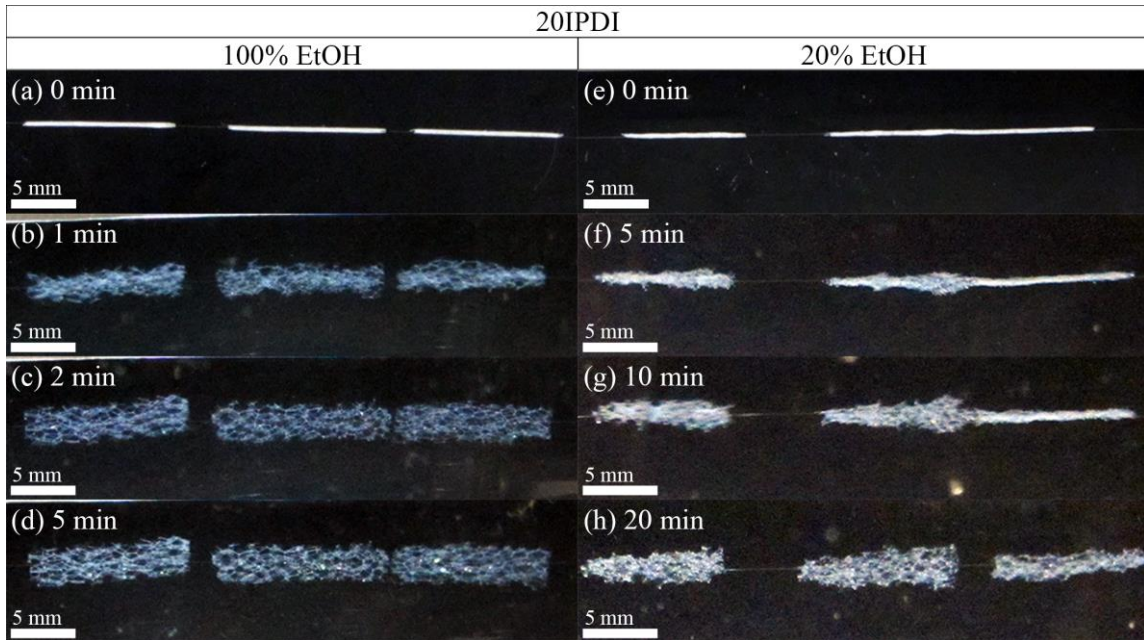
Figure 2.7: Images of 20IPDI actuation in 37 °C EtOH solutions. (a), (b), (c), and (d) show 20IPDI actuation in 100% EtOH at 0, 1, 2, and 5 min, respectively. (e), (f), (g) and (h) show 20IPDI actuation in 20% EtOH at 0, 5, 10, and 20 min, respectively.

Both swelling and shape memory effects are critical factors in the SMP foam volume recovery shown in this study. Previous studies on solvent-stimulated actuation have reported that the swelling of solvent into the polymer matrix changes the internal energy and decreases the relaxation time.[56,59] As shown in Figures 2.4, 2.5, and 2.6, all foam compositions exhibited swelling to greater than their original volumes during submersion in 100% solutions of both DMSO and EtOH. The rates of volume ratio increase during the swelling experiment and the volume recovery experiments are very similar for all foam compositions. However, while EtOH exposure resulted in an expected decrease in relaxation time and T_g (tan δ_{max}) values below 37 °C for all foam compositions, DMSO exposure did not cause the same result. Rather, as shown for 20IPDI in Figures

2.2, 2.4, and 2.5, DMSO exposure resulted in polymer swelling but minimal to no relaxation in DMA kinetic experiments. This suggests differing mechanisms through which DMSO and EtOH influence volume recovery. During swelling, solvent penetrates into the polymer matrix and separates the polymer chains, increasing overall volume and enabling viscous migration between polymer network and solvent.[59] During shape recovery, heating the polymer above T_{trans} increases chain mobility, allowing entropic forces to orient polymer chains from the organized state of the temporary shape to the disorganized state of the original shape.[30] This study suggests that DMSO exposure primarily causes volume change due to solvent swelling separating polymer chains, increasing volume, but stimulation of the conformational change and polymer chain orientation during shape recovery is less of a factor. Thus, both swelling and shape recovery influence volume recovery, but swelling may dominate the volume change that occurs without chain relaxation expected. However, EtOH exposure was observed to cause both volume change from swelling as well as relaxation during shape recovery. Thus, rapid volume recovery occurs as a result of both swelling and shape recovery as indicated by the expected chain relaxation.

We hypothesize that the mechanism and effectiveness of solvent-stimulated actuation is heavily dependent on the relative molecular interactions of the solvent and polymer backbone. In these studies, EtOH proved to be a much more effective plasticizer of the polyurethane-based SMP foams than DMSO and water. This is likely caused by two primary factors: (1) the solvent's ability to penetrate the SMP and plasticize the polymer backbone and (2) the availability of isocyanate species to plasticization and mobility. Lu

et al. demonstrated that submersion in EtOH decreased the T_g of polyurethanes as a function of time due to hydrogen bonding interactions between the solvent and the urethane linkages.[56] However, previous studies of solvent-stimulated actuation of polyurethanes reported opposite results to this study; namely, decreased shape recovery was observed with EtOH compared to water, which was attributed to stronger hydrogen bonding interactions between urethane linkages and water relative to those with EtOH.[38,56] These differing results reinforce that interactions between the chosen solvent and specific polymer chemistry are critical to the shape recovery effect. The SMP foam chemical compositions used in these studies were designed for increased hydrophobicity and decreased water plasticization, as reported by Hasan et al.[34] Methyl groups in the isocyanate monomers in combination with the ring structure of IPDI hinder water penetration into the polymer backbone, reducing available isocyanate linkages for water plasticization.[34] We hypothesize that the presence of both polar and non-polar regions in the EtOH molecule allow for drastically increased interactions with this polymer backbone compared to water and DMSO. Specifically, the OH functionality in the EtOH molecule will readily interact with urethane linkages while the C-C tail will interact with the non-polar regions of the isocyanates. Further investigation is required to fully characterize and understand the mechanisms underlying the solvent stimulated SMP foam actuation observed in this study.

2.4 Conclusion

Solvent-stimulated volume recovery of hydrophobic polyurethane-based SMP foams using DMSO and EtOH was shown. Dramatic decreases in Tg were observed with

exposure to water, DMSO, and EtOH. EtOH was shown to decrease SMP foam relaxation times to less than 1 min in DMA kinetic experiments. Furthermore, rapid shape recovery and volume swelling was observed for SMP foams in high concentrations of both DMSO and EtOH, as well as in decreased concentrations of EtOH. This study demonstrates effective control of SMP foam volume recovery using both DMSO and EtOH, including in aqueous environments, and that pairing of polymer composition and solvent selection is critical to the effectiveness of this actuation technique. Future work should investigate other solvents, as use of EtOH and DMSO are not ideal solvents in many applications, including biomedical applications due to moderate to severe toxicological effects.[46,47] However, this work serves as a proof of concept of SMP foam actuation control using non-water solvents and provides insight into mechanisms that can be investigated for future material and device design work. Overall, this work demonstrates great potential for use of solvents as an alternative actuation stimulant for polyurethane-based SMP foams and may improve feasibility of using SMP materials in a variety of applications.

CHAPTER III

IN VITRO AND *IN VIVO* EVALUATION OF A SHAPE MEMORY POLYMER FOAM-OVER-WIRE EMBOLIZATION DEVICE DELIVERED IN SACCULAR ANEURYSM MODELS[*]

3.1 Introduction

3.1.1 Endovascular Treatment of Intracranial Saccular Aneurysms

Intracranial saccular aneurysms typically develop at the apex of subarachnoid arterial bifurcations at the base of the brain.[3] Subarachnoid hemorrhage, primarily caused by ruptured intracranial aneurysms, affects approximately 1 in 10,000 Americans each year and is fatal in 35% to 50% of all patients.[3]

Standard endovascular treatment using bare metal coils involves delivering several platinum wire coils through a microcatheter into an aneurysm to occlude the aneurysm volume.[8,9] The treatment goal is for the packed coils to provide sufficient flow stasis to result in embolization of the aneurysm sac and neointima growth across the aneurysm neck. However, implanted bare platinum coils are prone to compaction, result in low volume occlusion ranging from 23-37%, and exhibit a recanalization rate of 21-34% with 13% requiring retreatment.[20,21,60-63] Minimal tissue response to the bioinert platinum coils stunts tissue healing, resulting in unorganized thrombus formation within the aneurysm sac that may not organize within 3 years following treatment.[19] Several devices, including

---

polymer embedded coils, have been investigated in order to improve upon bare platinum coiling outcomes. Bioactive and biodegradable polymer coated coils increase tissue response, but are susceptible to recanalization as the polymer is absorbed.[23] HydroCoils® (Microvention Inc., Tustin, CA) are platinum coils coated with a bioinert poly(acrylamide-co-acrylic acid) hydrogel with pores less than 10 µm in diameter.[52] The hydrogel swells in water, displacing blood as it fills the aneurysm volume, resulting in volume occlusion ranging 45-85%.[17,18,27] Although major recurrence has been reported to be lower when using HydroCoils®, the effect on long-term clinical outcomes is unclear.[28]

3.1.2 Proposed Shape Memory Polymer Foam Treatment

Shape memory polymers (SMP) exhibit the ability to maintain a temporary shape and subsequently recover their original shape in response to a thermal, chemical, or optical stimulus.[30] SMPs fabricated into a foam geometry are advantageous for endovascular embolization due to their large surface area to volume ratios that enable large volume transitions required for catheter delivery and subsequent aneurysm occlusion.[33] Biostable polyurethane SMP foams have been reported with 700-1000 µm pores, biocompatibility, and tunable thermal and mechanical properties for improved actuation control.[1,33] Unlike hydrogels, the large pores of SMP foam provide channels for blood flow and a scaffold for interconnected thrombus formation, cell infiltration, and tissue healing throughout the foam volume.[1,33]

Previous studies investigating saccular aneurysm occlusion using SMP foam documented excellent aneurysm occlusion, mild inflammatory response, and mature tissue healing.[1] However, these devices were designed for catheters too large for conventional

neurovascular applications, functionally different than standard coils, and not visible under fluoroscopy.

Therefore, a new device design was developed to provide a low adoption hurdle for clinicians familiar with standard coils and enable delivery through traditional microcatheters using fluoroscopy. The device design employs a SMP foam that is delivered to the aneurysm over a radiopaque nickel-titanium (nitinol) and platinum wire backbone, mechanically detached, and then actuated either passively using physiological conditions or using a laser heated injection. Devices were fabricated, tested in simulated actuation methods, and delivered to *in vitro* and *in vivo* saccular aneurysm models. Delivery and detachment efficacy, laser heating efficacy, aneurysm volume occlusion, and acute clotting were measured and evaluated during the studies.

3.2 Materials and Methods

3.2.1 Embolization Device Design and Fabrication

The embolization device system consisted of an SMP foam-over-wire (FOW) implant device and a cable tube delivery and detachment device with an optional laser heated saline injection for SMP foam expansion as shown in Figure 3.1.
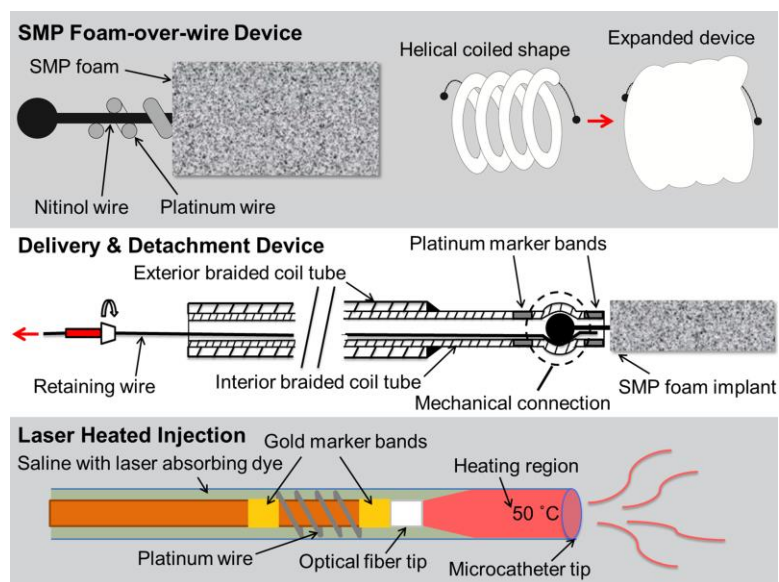
Figure 3.1: Schematic diagrams of the SMP foam-over-wire (top panel), the delivery and detachment device (middle panel), and the laser heating mechanism (bottom panel).

3.2.1.1 Shape Memory Polymer Foam-over-Wire Implant

The implant device consists of SMP foam secured around a platinum wound nitinol backbone wire (Figure 3.1, top panel). N,N,N′,N′-Tetrakis(2-hydroxypropyl)ethylenediamine (HPED, 99%), triethanolamine (TEA, 98%), trimethyl-1,6-hexamethylene diisocyanate, 2,2,4- and 2,4,4- mixture (TMHDI), and deionized (DI) water (> 17 MΩ cm purity) were used as received to synthesize SMP foams using protocol reported previously.[41] Under sonication, 8 mm SMP foam cylinders were chemically etched in 0.1 M hydrochloric acid, cleaned using isopropyl alcohol and detergent, and then rinsed with reverse osmosis (RO) water. Cleaned foam cylinders were dried overnight in an oven at 50 °C under vacuum.

The platinum-nitinol wire backbone was annealed over a mandrel in a furnace to set a helical shape, quenched in water, and cleaned using isopropyl alcohol. SMP foam cylinders were cut from the cleaned and dried cylinders using a 2.5 mm diameter biopsy punch blade adhered to the end of a 2.97 mm ID stainless steel tube and the wire backbone was threaded axially through the SMP foam (Figure 3.2A). Devices were fabricated with both 2 cm and 4 cm total lengths of SMP foam. The implant devices were held taught and the SMP foam was radially compressed (Figure 3.2B) using a heated SC250 Stent Crimper (Machine Solution Inc.®, Flagstaff, AZ). Medical grade UV-cure epoxy was used to secure the compressed SMP foam at each end of the device.
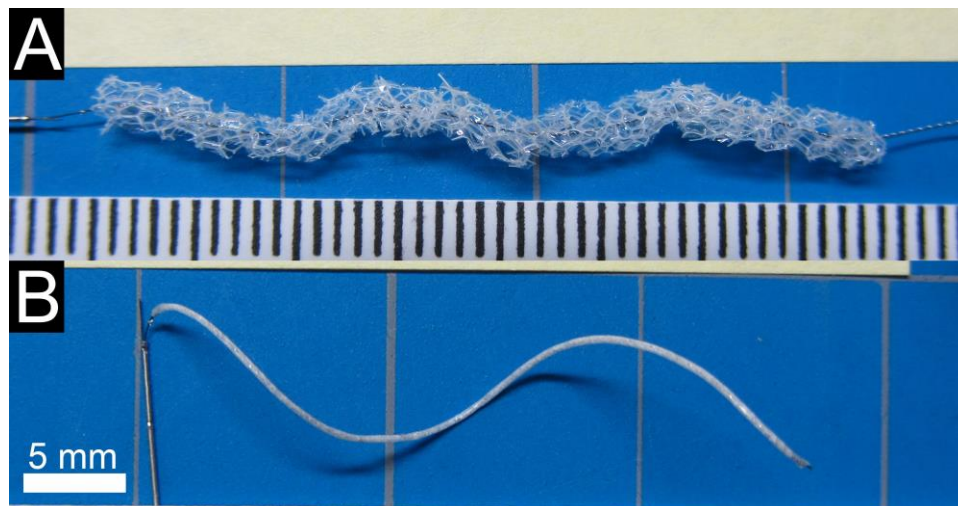
Figure 3.2: FOW embolization device. A) The threaded device prior to radial compression and attachment to the delivery and detachment device. Scale is mm. B) The assembled embolization device with compressed FOW device attached to the delivery and detachment device.

3.2.1.2 Delivery and Detachment Device

The braided coil assembly (Figure 3.1, middle panel) consisted of a 0.31 mm OD stainless steel ACTONE^{TM} cable tube (Asahi Intecc Co., Aichi, Japan) reinforced with a 0.46 mm OD stainless steel ACTONE^{TM} cable tube for distal flexibility and reinforced proximal pushability. A nitinol retention wire was passed through the entire length of the braided coil assembly. A laser welding system was used to secure a platinum marker band 4 mm from the distal tip of the braided coil assembly. A ball tip was created on each end of the implant using the laser welder and the ball tip was press-fit into the distal tip of the delivery system on top of the retaining wire, causing the braided coil to distend and apply a spring force on the ball tip. A second platinum marker band was laser welded at the distal tip of the delivery system to constrain the implant ball tip. The assembled devices were individually sealed in a sterilized pouch with desiccant and, for the *in vivo* studies, sterilized by ethylene oxide and allowed to degas for 24 hours.

3.2.1.3 Laser Heater Device and Injection

Fiber optic cables were fabricated using 200/220/239 µm core/cladding/buffer optical fiber and connectorized with 230 µm ST epoxy fiber connectors. Reinforced furcation and polytetrafluoroethylene tubing segments were placed over the proximal 30 cm of the fiber. Gold marker bands were epoxied to the optical fiber at the distal tip and 2 cm proximal to the distal tip using medical grade thermal cure epoxy. Two platinum wires were laser welded to opposite sides of the marker bands and wound around the fiber. The injected solution consisted of phosphate buffered saline doped with indocyanine green (ICG) at a concentration of 375 µM. The concentration was chosen to achieve a

penetration depth of approximately 300 µm by interpolating data collected by Landsman et al.[64] A full schematic of the laser heated injection is shown in the bottom panel of Figure 3.1.

3.2.2 In vitro Device Studies

3.2.2.1 SMP Foam Actuation

SMP foam actuation was characterized using simulated passive and active actuation methods. FOW devices were submerged in 37 °C RO water to simulate passive actuation and imaged at 2 min interval to 20 min and 5 min interval to 60 min total submersed time. To simulate active actuation, devices were submerged in 37 °C RO water for 5 min, then submerged in 50 °C RO water and imaged at 1 min interval to 15 min total submersed time. Imaging software was used to measure the foam diameter at 5 points along the length of each sample at each time point.

3.2.2.2 Aneurysm Model Fabrication and Flow System

An aneurysm model consisting of a 10 mm diameter sphere embedded in the side of a 5 mm diameter cylinder was designed in CAD software, printed using a fused deposition modeling system, and smoothed using sandpaper. Sylgard 184 polydimethylsiloxane (PDMS, Dow Corning Corp., Midland, MI) was cast and cured around the model, and the printed model was dissolved using a heated base bath.

During testing, the PDMS aneurysm model was inserted in a flow loop as shown in Figure 3.3. Heated RO water was siphoned into a bath with the aneurysm model to maintain isothermal conditions at 37 °C. One peristaltic pump was used to maintain the water level above the submerged aneurysm model. A second peristaltic pump and pulse

dampener supplied steady flow through the parent artery of the PDMS aneurysm model at approximately 240 mL/min to match the Reynold's Number of human common carotid artery peak blood flow rates reported by Holdsworth et al.[65] A needle thermocouple was placed through a small port at the aneurysm dome to monitor temperature during setup and removed prior to device delivery.
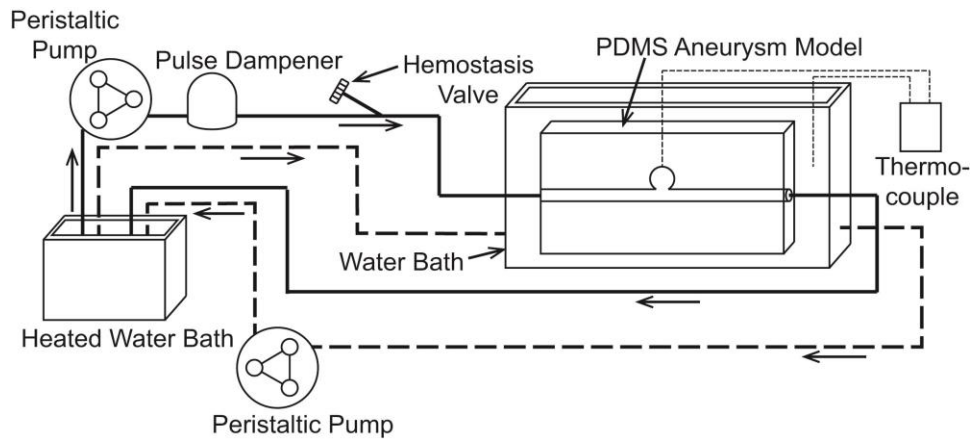
Figure 3.3: *In vitro* **flow system schematic. The solid line indicates the simulated artery flow through the PDMS aneurysm model. The dashed line indicates the isothermal bath flow.**

3.2.2.3 Embolization Device Delivery and Evaluation

Multiple FOW embolization devices were delivered via microcatheter into the aneurysm model. A 2.8/2.3 F proximal/distal microcatheter with a 0.53 mm lumen was navigated to the aneurysm using a guidewire. For each device, a hemostasis valve was used to secure a stainless steel hypotube introducer and the devices were advanced through the microcatheter to the aneurysm. Each device was positioned into the aneurysm such

that the entire implant device was contained inside the aneurysm and the proximal platinum band at the distal tip of the delivery and detachment device was out of the microcatheter. The retaining wire on the delivery and detachment device was removed proximally and the cable tube was retracted into the microcatheter for complete release of the implant. The SMP foam passively actuated in the 37 °C water after implantation. Multiple devices were inserted into the aneurysm until the aneurysm was considered sufficiently occluded. Occlusion was indicated by qualitative visualization of extended dwell time or prevention of dye infiltrating the aneurysm. Theoretical volume occlusion (TVO) was calculated using Equation 3.1,

$$TVO = \frac{V_f}{V_a} = \frac{\pi\left(\frac{D_f}{2}\right)^2 L_f}{\frac{4}{3}\pi\left(\frac{D_a}{2}\right)^3} \tag{3.1}$$

where V_f is expanded foam volume, V_a is the aneurysm volume, D_f is the expanded foam diameter, L_f is the total foam length, and D_a is the aneurysm diameter. The TVO calculation assumes the aneurysm is spherical and the SMP foam is a uniform cylinder of 1.25 mm diameter.

3.2.2.4 Laser Heater Characterization

Laser heater characterization was performed by recording the temperature of the aneurysm dome during heated injection in an *in vitro* flow loop similar the one shown in Figure 3.3. A microcatheter was passed through a hemostasis valve to the aneurysm dome. The optical fiber was inserted through a Y-adapter hemostasis valve and the tip was positioned approximately 2 cm proximal to the distal tip of the catheter. The ICG solution was injected using a syringe pump through the Y-adapter on the microcatheter. Systemic

flow was discontinued and the ICG injection was initiated at a flow rate of 1.5 mL/min. An 808 nm continuous wave diode laser was activated to emit radiation at approximately 1.9-2 W. The temperature in the dome of the aneurysm was measured every ten seconds for two minutes. Three devices were used and three injections were characterized for each device.

3.2.3 In vivo Device Study

3.2.3.1 Porcine Sidewall Saccular Aneurysm Model Creation

Animal studies were conducted in accordance with policies set by the Texas A&M University Institutional Animal Care and Use Committee, and met all federal requirements as defined in the Animal Welfare Act, the Public Health Service Policy, and the Humane Care and Use of Laboratory Animals. Additionally, studies observed NIH guidelines (or for non-U.S. residents similar national regulations) for the care and use of laboratory animals (NIH Publication #85-23 Rev. 1985).

Animal studies were performed in the catheterization laboratory at the Texas A&M Institute for Preclinical Studies. Fluoroscopic visualization was achieved using the Allura Xper FD20 system (Koninklijke Philips N.V., Eindhoven, The Netherlands). A saccular sidewall vein pouch aneurysm model created in a 3-4 month old, 30-40 kg Yorkshire swine using a previously described model.[66] Study subjects were premedicated with Telazol 5 mg/kg and 0.01 mg/kg buprenorphine administered intramuscularly. Following endotracheal intubation, study subjects were mechanically ventilated and maintained on isoflurane. Using sterile technique, a 10 cm incision was made in the ventral cervical midline and using a combination of sharp and blunt dissection the external jugular vein

45

and carotid arteries were isolated. A 4 cm long segment of the external jugular vein was isolated, excised, and divided transversely to create two 2 cm open-ended pouches. The common carotid arteries were cleaned of adventitia, and vascular clamps placed at each end of the target area on the artery. A 3-4 mm arteriotomy was created and an end-to-side anastomosis of the venous pouch to the carotid artery performed using 7-0 polypropylene sutures. A 6-9 mm diameter aneurysm was created on each common carotid artery of two animals for a total of four aneurysms. After hemostasis was confirmed, the subcutaneous tissues were loosely closed.

3.2.3.2 Embolization Device Delivery and Angiographic Evaluation

Each aneurysm was accessed via endovascular technique for device delivery and implantation. A 6 F intravascular sheath was inserted percutaneously into the femoral artery with ultrasound guidance and a 5 F guide catheter was inserted through the introducer. Using fluoroscopic guidance, the guide catheter was advanced over a guidewire to the proximal right or left carotid artery proximal to the aneurysm. Digital subtraction angiography with 3-D reconstruction angiography was performed to fully characterize each aneurysm. A 2.8/2.3 F proximal/distal microcatheter with 0.53 mm lumen was navigated to the aneurysm using a guidewire. Multiple FOW embolization devices were delivered through microcatheters and deployed in each aneurysm under fluoroscopic guidance. Devices were delivered and detached using the same methods used during *in vitro* studies. After implantation, the SMP foam passively expanded in the physiological conditions. Additional devices were inserted into the aneurysm until the aneurysm was considered sufficiently occluded. Implant time was measured per aneurysm

as the time between entry of the first device into the microcatheter and detachment of the final device. Adequacy of occlusion was determined qualitatively by visualization of extended dwell time or prevention of dye infiltrating the aneurysm. TVO was calculated using Equation 1, where D_a was the aneurysm diameter averaged from four measurements taken from angiographic images obtained using various angles, with the same assumptions as conducted for *in vitro* studies.

3.2.3.3 Laser Heated Injection

The laser heated injection was used in one aneurysm after implantation with FOW devices to accelerate and increase expansion of the SMP foam. The laser heating device was positioned using the same methods used during *in vitro* studies. A second 6 F introducer was inserted into the femoral artery on the opposite side of the previous introducer. A 5 F balloon catheter was inserted through the second introducer and positioned proximal to the aneurysm site adjacent to the guide catheter. The balloon catheter was inflated to prevent blood flow to the aneurysm and ICG-doped saline was injected at 1.5 mL/min through the microcatheter. The same laser used for *in vitro* studies was activated for 2 min during injection. After injection, the balloon catheter was deflated and angiography was performed to confirm aneurysm integrity and assess any change in aneurysm occlusion.

3.2.3.4 Ex vivo Evaluation

After implantation and angiographic imaging of both aneurysms in each animal, the animal was sacrificed and the aneurysms explanted and rinsed in saline. The parent artery was divided axially and the aneurysm neck was exposed and imaged. The aneurysm

wall was opened and the implanted devices were imaged within the aneurysm sac and after removal from the aneurysm to evaluate implant device stability, aneurysm occlusion, and clotting.

3.3 Results

3.3.1 In vitro Device Studies

3.3.1.1 SMP Foam Actuation

As shown in Figure 3.4, SMP foam submerged in 37 °C RO water actuated to an average diameter less than 0.53 mm after 5 min, 1.26 mm after 30 min, and 1.44 mm after 60 min. After 5 minutes of submersion in 37 °C RO water, SMP foam submerged in 50 °C RO water actuated to an average diameter of 1.02 mm within 1 min and 1.65 mm after 10. Three samples were tested per actuation method.
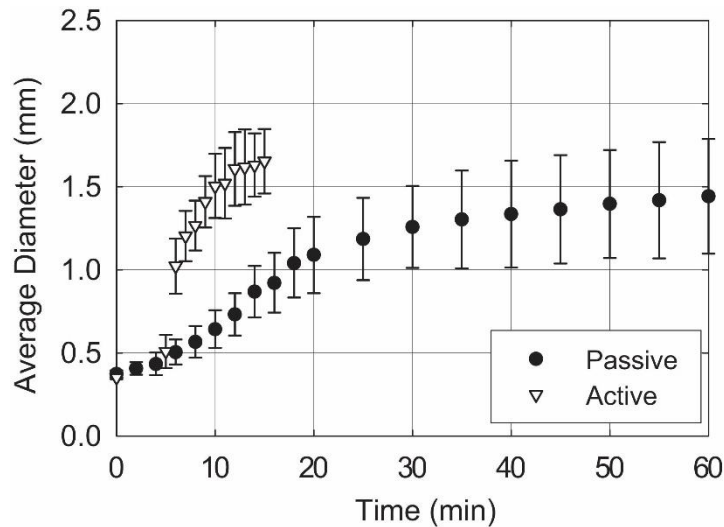
Figure 3.4: SMP foam expansion using simulated passive and active actuation methods.

48

3.3.1.2 Embolization Device Delivery

The spherical aneurysm model was fabricated with a dome diameter of 9.79 ± 0.12 mm and a neck diameter ranging 2.09-6.81 mm. Embolization device delivery into the aneurysm model is shown in Figure 3.5. Four FOW devices 4 cm in length were delivered to the aneurysm model. Two of four implant devices were detached without complication, whereas two devices detached in the microcatheter during repositioning and were successfully deployed using a guidewire. All four devices were implanted into the aneurysm model without migration into the parent vessel. TVO was calculated to be 40%.
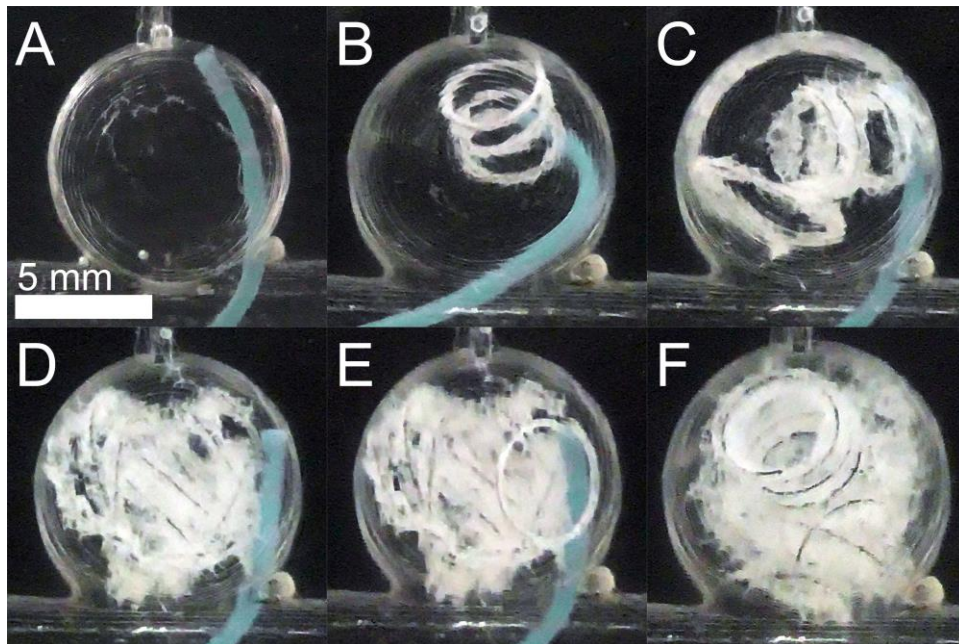
Figure 3.5: FOW device *in vitro* delivery. A) Aneurysm model prior to device delivery. B-E) Delivery of four devices into the aneurysm model. F) Aneurysm model is well occluded.

3.3.1.3 Laser Heater Characterization

The conducted *in vitro* tests showed that three of the tested devices increased the aneurysm dome temperature to at least 49 °C after 1-1.5 minutes of injection.
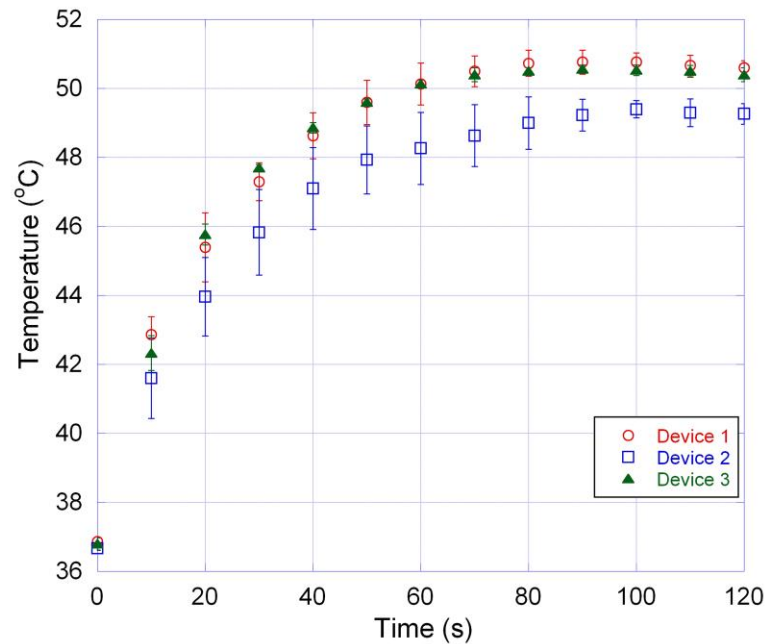
Figure 3.6: Heating profile of three different laser heating devices each tested three times.

3.3.2 In vivo Device Study

3.3.2.1 Embolization Device Delivery and Angiographic Evaluation

After aneurysm formation, three of four aneurysms exhibited good stability via angiography, while one aneurysm showed hemorrhage at the anastomosis site. All four aneurysms were successfully treated with FOW embolization devices with an average implant time of 65.0 ± 16.4 min. Figure 3.7 summarizes angiographic evaluation of each

aneurysm before and after treatment. All treated aneurysms exhibited significant occlusion, particularly at the dome apex, with reduced contrast infiltration into the aneurysm. Hemorrhage at the anastomosis site shown in panel D.1 is no longer seen after treatment as shown in panel D.2. The minimal TVO calculated for the four aneurysms was 72% (Table 3.1).

Table 3.1: Aneurysm model and device dimensions and TVO values

Aneurysm Label	Aneurysm Diameter (mm)	Neck Diameter (mm)	No. Devices	Total Device Length (cm)	Theoretical Volume Occlusion
A	8.66 ± 1.45	4.42	6	20.0	72%
B	7.45 ± 1.11	4.63	4	16.1	91%
C	7.78 ± 1.91	4.42	6	14.9	74%
D	5.74 ± 0.77	3.40	3	11.4	141%
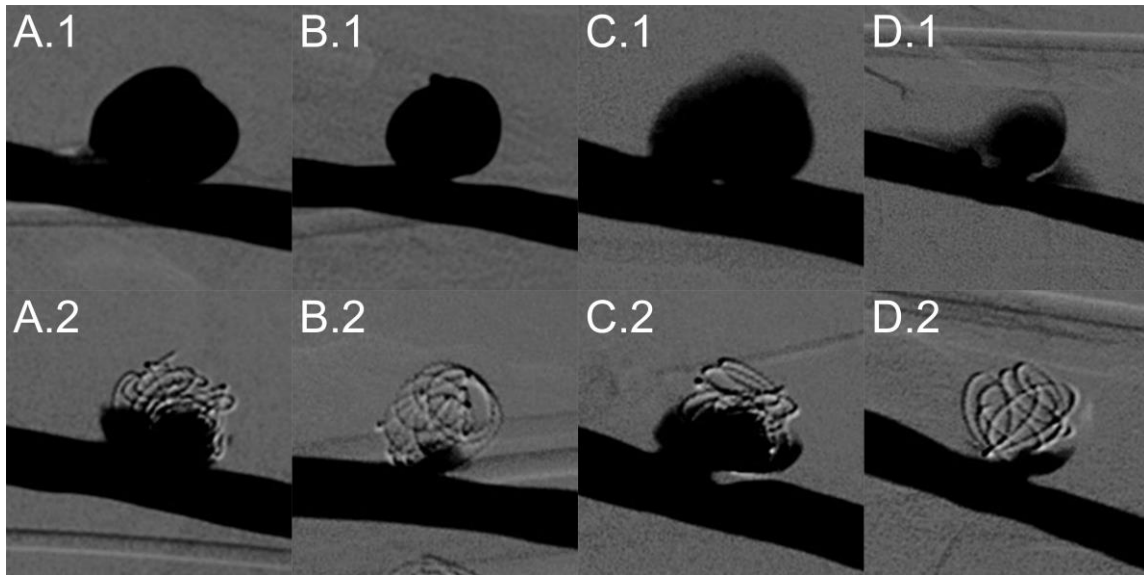
Figure 3.7: FOW device treatment of porcine sidewall aneurysms labeled A, B, C, and D. Top Row: Digital subtraction angiography prior to device implantation. Bottom Row: Digital subtraction angiography after implantation of FOW devices.

Embolization devices were delivered and implanted in the aneurysms with minimal complications. All device components were clearly identified under fluoroscopy. 19 of 26 (73%) FOW devices inserted into the microcatheter were successfully implanted in aneurysms, two devices could not be packed into aneurysms that had already occluded, and five devices could not be advanced due to excessive device expansion within the catheter. Delivery and detachment of devices was successfully performed in 24 of 26 (92%) attempts with both complications being detachment of the implant during repositioning. One detached device was delivered to the aneurysm using a guidewire and the other was partially packed in the aneurysm and subsequently removed using an endovascular snare system. As shown in Figure 3.8, the laser heated injection was

conducted without complication and no acute adverse reactions were detected. Minimal

reduction in contrast infiltration was observed following the laser heated injection.
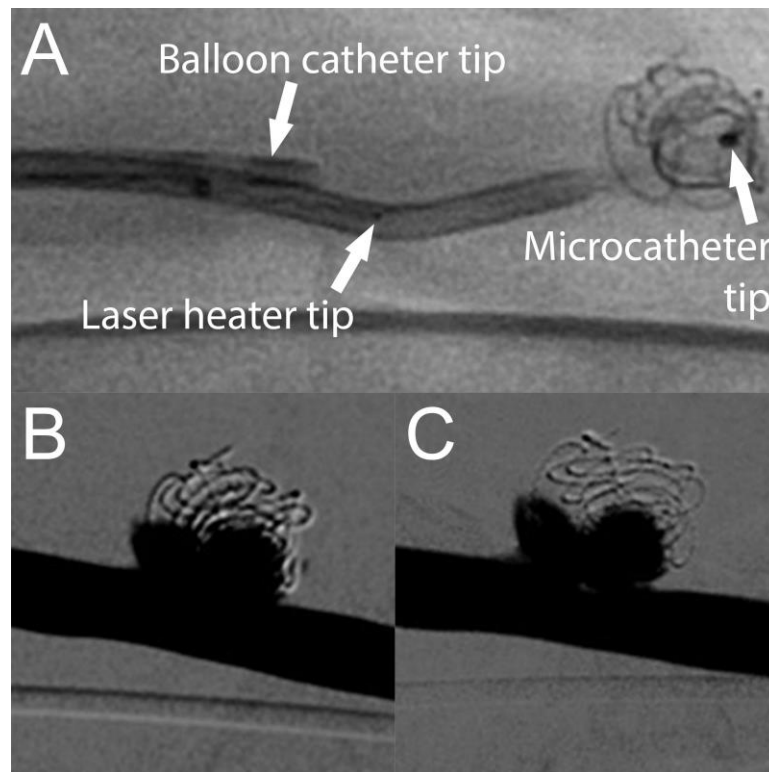
Figure 3.8: Laser heated injection for increased SMP foam expansion. A) Fluoroscopic image prior to balloon inflation and ICG-doped saline injection. Digital subtraction angiography of treated aneurysm prior to (B) and after (C) laser heated injection.

3.3.2.2 Ex vivo Evaluation

The explanted aneurysms showed no device perforation through the aneurysm wall

and excellent thrombus formation throughout the implanted FOW devices. Figure 3.9

shows an explanted aneurysm and the aneurysm content of implanted devices and

thrombus. All aneurysms were explanted within 3 hours after final device implantation in each aneurysm.
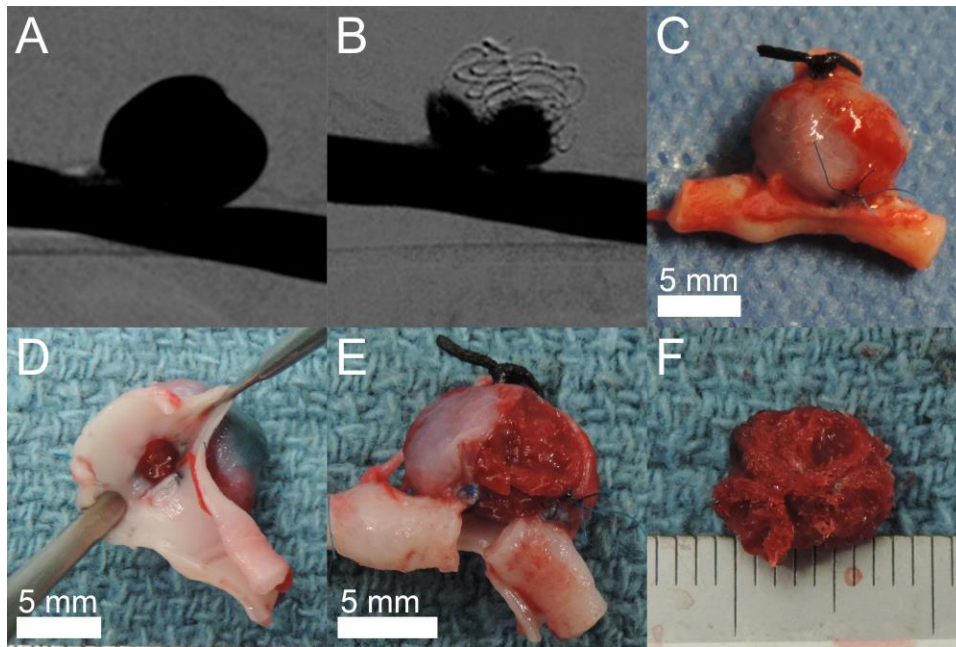
Figure 3.9: Explanted porcine sidewall aneurysm model. A) Digital subtraction angiography of the aneurysm prior to treatment. B) Digital subtraction angiography of the aneurysm after implantation of four FOW devices. C) Explanted aneurysm including parent vessel. D) Visualization of the explanted aneurysm neck. E) Partial removal of the explanted aneurysm wall. F) Thrombus with the implanted devices is stable after removal from the aneurysm. Scale is mm.

3.4 Discussion

The primary goal of these studies was to evaluate the efficacy of FOW embolization devices for endovascular treatment of saccular aneurysms. The devices were tested using *in vitro* and *in vivo* saccular aneurysm models to measure and evaluate

delivery and detachment efficacy, laser heating efficacy, aneurysm volume occlusion, and acute clotting.

Passive SMP foam actuation indicated a 5 min working time, during which time the foam is smaller than the delivery microcatheter ID (0.53 mm). This is equal to published repositioning times of the HydroCoils®.[27] However, the foam diameters of 1.26 mm at 30 min passive actuation and 1.02 mm at 1 min active actuation are both greater than reported expanded diameter of HydroCoils® of 0.69 mm, indicating higher occlusion per device length of the FOW compared to HydroCoils®.[27]

The embolization device delivery *in vitro* demonstrated excellent positioning of multiple devices in the saccular aneurysm model with no device protrusion or migration into the parent vessel (Figure 3.5). The device detachment success rate of 50% revealed a need for increased grip strength and consistency in fabrication, both of which were implemented for devices fabricated for the *in vivo* study. Theoretical volume occlusion (TVO) of the *in vitro* study was lower than expected due to limited total device length of 16 cm relative to the large aneurysm diameter, but still resulted in greater than reported volume occlusion values for bare platinum coil treatments.[60,61]

All three laser heating devices increased the temperature (Figure 3.6) in the aneurysm dome during *in vitro* studies to a temperature 10 °C greater than the published SMP foam transition temperature for successful SMP foam actuation.[41] Heating profile variation could be due to device imperfections or variation in the connector alignment and fiber tip location in the catheter.

Post treatment angiography during the *in vivo* study shown in Figure 3.7 exhibited complete elimination of flow into the aneurysm dome apex and substantial reduction of flow near the aneurysm neck in all 4 aneurysm models. FOW devices treated all porcine aneurysms with an average total device length of 15.6 cm, which is less than the average values reported when using bare platinum coils (52-53 cm) or HydroCoils® (31-38 cm) in similar sized aneurysms. Additionally, FOW device treatments resulted in TVO ranging 72-141%, which is equal to or greater than those reported by bare platinum coils (29-31%) or HydroCoils® (76-86%) in similar sized aneurysms.[17,18] However, the aneurysm D value (Table 1) may be falsely high due to angiography measurements underestimating the actual diameter of the aneurysm possibly due to incomplete contrast filling due to the anastomosis hemorrhage of aneurysm D (Figure 3.7 D.1) before treatment. The porous structure and low radiographic contrast of the SMP foam enables contrast agent to infiltrate the foam and be visualized under fluoroscopy. Therefore, the absence of contrast agent flow into the aneurysm indicates complete thrombus formation within the implanted SMP foam. This is drastically different compared to treatments with bare platinum coils that saturate the aneurysm space with radiographic contrast, preventing visualization of any infiltrating contrast agent, and with HydroCoils® that displace blood from the aneurysm with hydrogel.[17] In those cases, occlusion by thrombus formation cannot be reliably assessed *in vivo*. Thrombus formation within the porcine aneurysm models was confirmed by evaluation of the explanted aneurysms as shown in Figure 3.9. All aneurysm contents exhibited stable thrombus formation throughout the implant device mass. The formation of stable thrombus is an early and critical step in the inflammation response that

has been shown to promote fibrous connective tissue formation within implanted SMP foams. The pore interconnectivity of the SMP foam enables connective tissue integration throughout the device volume within 30 days.[1] This differs from occlusion with platinum coils that may not result in organized thrombus within 3 years or with HydroCoils® that show tissue deposition within 2-6 weeks around the devices, but little to no integration within the hydrogel due to the pore size.[17,19] The thrombus formation throughout the explanted aneurysm mass also suggests that flow penetrating into two of the four treated aneurysms is an artifact of the 2D imaging overlaying flow around the outside of the ball of implanted contents.

Embolization devices were implanted with stable positioning of multiple devices in each saccular aneurysm model. Implant times for FOW devices were longer than reported average procedure times for platinum coils (27 min) and HydroCoils® (28 min) due to device complications.[17] Implant devices had a moderate success rate with complications of increased delivery friction due to foam expansion in the microcatheter indicating a need for increased foam hydrophobicity to delay passive expansion.[41] Detachment devices were able to deliver, reposition, and retract almost all devices without complication. The two detachment device complications were the direct result of either a fully packed aneurysm preventing device delivery or undesired SMP foam expansion and can be addressed without a detachment design change. The laser heating injection resulted in minimal decrease of contrast infiltration in the treated aneurysm, indicating either complete passive expansion of SMP foams or that the temperature increase was not

sufficient to increase SMP foam expansion. However, no negative acute effects were observed as a result of the laser heating.

3.5 Conclusions

In conclusion, the FOW embolization device design combines the filling and surface area advantages of SMP foam with fluoroscopic contrast and mechanical stability of metal coils, providing a low adoption hurdle for clinicians experienced with coil devices. Furthermore, the *in vitro* and *in vivo* studies show great promise for the efficacy of the FOW embolization device for endovascular treatment of intracranial saccular aneurysms.

CHAPTER IV

IN VITRO AND *IN VIVO* PERFORMANCE OF A SHAPE MEMORY POLYMER

FOAM-COATED COIL EMBOLIZATION DEVICE

4.1 Introduction

Aneurysmal subarachnoid hemorrhage (aSAH), bleeding into the subarachnoid space in the brain due to intracranial aneurysm rupture, is marked by significant morbidity and mortality rates. Incidence of aSAH occurs in 9.7 – 14.5 out of every 100,000 adults in the United States where at least 25% of patients die and approximately 50% of survivors are left with persistent neurological deficit.[4] Standard endovascular treatment of intracranial saccular aneurysms involves the delivery and implantation of embolization coil devices into the aneurysm to promote thrombus formation, tissue healing, and neointimal growth across the aneurysm neck.[7] However, aneurysm recurrence after endovascular coiling occurs in 20.8% of cases, requiring retreatment in 10.3% of cases.[12] Diminished packing density, which is the ratio of implanted device volume to aneurysm volume, as well as poor or unstable thrombus organization have been associated with increased recurrence, among other mechanisms.[14-16] Polymer-embedded coils, including poly(glycolic acid) and hydrogel-coated coils, were introduced to increase packing density or improve thrombus organization but have not resulted in significantly improved long-term clinical outcomes.[26,28] Therefore, the need still exists for an embolization device capable of increasing packing density and improving thrombus organization.

Shape memory polymer (SMP) foams have been proposed as an advantageous biomaterial for endovascular embolization applications due to their shape recovery

capability and interconnected, large surface area porosity.[1,31,67] Thermo-responsive SMP foams are capable of being programmed to hold a temporary shape until stimulated by heat, at which time they recover their original shape.[29,33] SMP foams have been reported with increased angiographic occlusion, more advanced healing marked by mature connective tissue, and a thicker neointima layer compared to bare metal coils in porcine saccular aneurysm models.[1,31] Though both SMP foams and hydrogels exhibit volume-filling capability, SMP foams exhibit interconnected pores with diameters in the hundreds of microns, compared to hydrogel pore sizes less than 10 µm in diameter.[33,52] This interconnected porosity of the SMP foams acts as a scaffold for blood flow, thrombus formation, and tissue healing throughout the material volume.[1,31]

A prototype embolization device was previously designed using radially expanding SMP foam over a nickel-titanium (nitinol) and platinum wire backbone and demonstrated to have stable angiographic occlusion and clot formation in a porcine saccular aneurysm model.[67] However, the device exhibited some limitations including restricted working time, i.e. time allowed to deliver and reposition the device, and excessive stiffness that increased packing difficulty. To address these limitations, a SMP foam-coated coil (FCC) embolization device was designed utilizing SMP foam over a platinum alloy coil with nitinol core wire. The FCC device is designed to interface with a delivery wire and electrolytic detachment system similar to systems previously used with commercial devices. This study evaluated selected performance and biocompatibility characteristics of the implant device, including ease of delivery and working time through

physiologically simulated tortuous flow models and cytocompatibility, to assess feasibility of the device for clinical treatment of intracranial saccular aneurysms.

4.2 Materials and Methods

4.2.1 Device Fabrication

The foam-coated coil (FCC) device is composed of shape memory polymer (SMP) foam placed over a platinum-tungsten coil with nickel-titanium (nitinol) core wire. Trimethyl-1,6-hexamethylene diisocyanate, 2,2,4- and 2,4,4- mixture (TMHDI, TCI America Co., Portland, OR), N,N,N′,N′-Tetrakis(2-hydroxypropyl)ethylenediamine (HPED, 99%, Sigma-Aldrich Co., St. Louis, MO), triethanolamine (TEA, 98%, Sigma-Aldrich Co., St. Louis, MO), and deionized (DI) water (> 17 MΩ cm purity) were used as received to synthesize SMP foam as previously reported by Hasan et al.[34] Helical shaped coil assemblies composed of nickel-titanium wire inserted through the lumen of a platinum-tungsten coil were used as received (Heraeus, Hanau, Germany). For each device, SMP foam was cut into cylinders using a 1 mm diameter biopsy punch, and the coil assembly was threaded through the foam cylinder axis. A single leading coil loop was left uncoated by SMP foam at the distal end. The SMP foam cylinder was saturated with a 4 vol% solution of TMHDI, HPED, and TEA in tetrahydrofuran (THF, anhydrous, EMD Millipore Co., Darmstadt, Germany) and then cured by temperature ramp up to 120 °C at 20 °C/hr and held at 120 °C for 2 hr. The resulting SMP coating adheres the foam to the coil. Under sonication, the devices were cleaned using reverse osmosis (RO) water and isopropyl alcohol (IPA) and then dried at 100 °C for 12 hr under vacuum. SMP foam was heated to approximately 100 °C and radially compressed around the coil using a SC250

stent crimper (Machine Solutions Inc., Flagstaff, AZ) to 0.016 ± 0.001 inches (0.41 ± 0.03 mm) in diameter. FCC devices were fabricated with a helical diameter of 6 mm and straight length of 10 cm (6x10), a helical diameter of 4 mm and straight length of 6 cm (4x6), or a straight length of 20 cm (0x20). The devices were placed into a 0.022 inch (0.56 mm) inner diameter (ID) polytetrafluoroethylene (PTFE) tubing for storage and use as an introducer sheath.

For tests using microcatheters, devices were attached to delivery wires. Delivery wires were removed from various sized GDC® embolization coils (Stryker Co., Kalamazoo, MI) and attached to the proximal (clinician side) end of the FCC using 203A-CTH-F UV-cure epoxy (Dymax Co., Torrington, CT). Figure 4.1 shows a foam-coated coil device before and after radial compression.
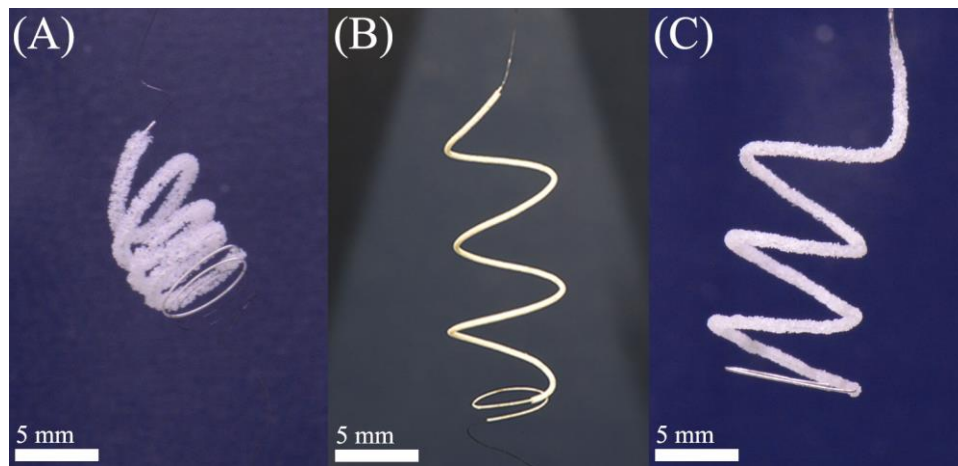
Figure 4.1: SMP foam-coated coil embolization device. (A) FCC device, 6x10 size, prior to radial compression. (B) FCC device, 6x10 size, after radial compression. (C) FCC device, 6x10 size, after expansion in 37 °C water for 30 min.

4.2.2 Shape Recovery

SMP foam expansion rate was characterized in an aqueous environment. FCC devices, 6x10 size, were straightened and submerged in 37 ± 0.2 °C RO water. Images were taken at 1 min intervals to 10 min total time submerged and at 5 min intervals to 30 min total time submerged. Foam diameter was measured at 5 different locations along each sample length for each time point using ImageJ software (NIH, Bethesda, MD).

4.2.3 Microcatheter Tip Deflection

Change in microcatheter tip angle during device deployment was measured to assess device stiffness. A 0.022 inch (0.56 mm) ID Trevo Pro 18 microcatheter (Stryker Co., Kalamazoo, MI) was steam shaped into a 110° angle with a 1 mm radius of curvature and secured in place. The starting tip angle was measured prior to each sample test from the image using ImageJ software.

Tip deflection was measured for FCC devices, 6x10 size, with delivery wire and GDC-18 2D devices (Stryker Co., Kalamazoo, MI) as controls. Samples were introduced into the microcatheter hub and advanced until the device distal tip was 2 cm proximal to the microcatheter tip. The delivery wire was clamped in an Insight 30 material tester system (MTS) (MTS Systems Co., Eden Prairie, MN) proximal to the microcatheter hub. The MTS advanced the device 0.5 cm through the microcatheter, and an image was taken. This was repeated until 5 cm was deployed out of the microcatheter. The tip angle was measured in each test image using ImageJ software and subtracted from the starting tip angle in order to calculate the tip deflection angle.

4.2.4 Ease of Delivery and Working Time

Ease of delivery and working time were evaluated on FCC devices through a tortuous path with physiologically simulating flow. Tubing with 2.38 mm ID was secured into a tortuous path with radii of curvature and curve angles based on a model reported by Sugiu et al. and as shown in Figure 4.2.[68] DI water was heated and pumped through the tubing at average flow rate of 44 ± 2 mL/min. Flow rate was calculated by matching the *in vitro* system Reynold's number to *in vivo* measurements of the middle cerebral artery reported by Reymond et al.[69] Inlet and outlet temperatures were maintained at 37 ± 1 °C. A 0.022 inch (0.56 mm) ID Trevo Pro 18 microcatheter was passed through the tortuous path until the microcatheter tip was past the tortuous path and held in 6.35 mm ID tubing. DI water was flushed through the microcatheter at 0.4 mL/min using a syringe pump.
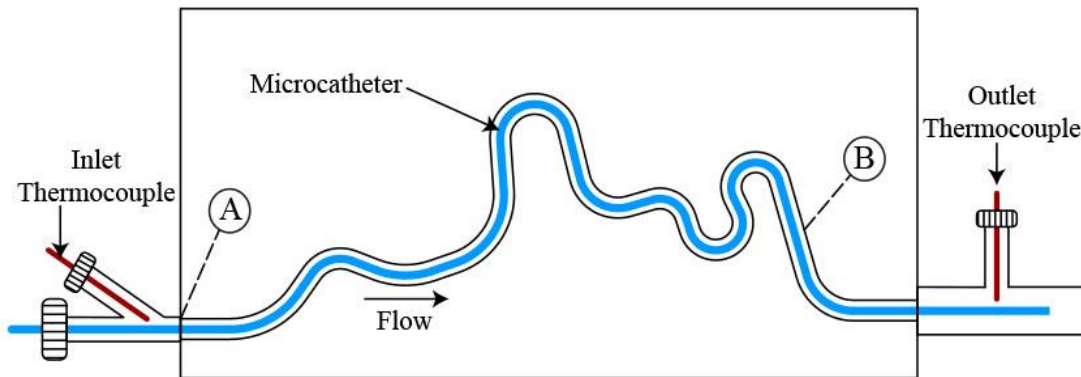
Figure 4.2: Tortuous path for ease of delivery and working time testing. The distal tip of the FCC implant is placed at (A) the entry of the tortuous path to start ease of delivery testing. The device is advanced until the junction to the delivery wire reaches (B) to end ease of delivery testing.

Ease of delivery was assessed for FCC devices, 6x10 size, attached to delivery wires with GDC-18 2D devices as controls. Devices were introduced into the microcatheter, and a timer was started. Devices were then advanced until the distal tip of the device was flush with the start of the tortuous path. The delivery wire was secured vertically and clamped 30 cm proximal to the microcatheter hub using a MTS with 50N load cell. Delivery force, the force experienced by the clinician during a procedure, was measured as the device was advanced 29 cm at 14.5 cm/min until the device tip was flush with the microcatheter.

Working time was then assessed for FCC devices following ease of delivery testing. The delivery wire was re-clamped in the MTS 6 cm proximal to the microcatheter hub. The delivery force was then measured as the device was deployed 5 cm out and retracted 5 cm at 10 cm/min to simulate repeated device repositioning. The deploy/retract cycle was repeated until an end point was observed: a successful retraction after the total submersion time exceeded 10 min, or mechanical damage was observed during a retraction cycle. A submersion time threshold of 10 min was chosen based on SMP foam shape recovery testing. Once an end point was reached, the total submersion time was recorded as the working time.

4.2.5 Cytocompatibility

A neutral red uptake test was performed on FCC devices to assess cytocompatibility. Dulbecco's modified eagle medium (DMEM; VWR, Radnor, PA), penicillin/streptomycin (P/S, 1%; VWR, Radnor, PA), newborn calf serum (NBCS, 10%; Sigma-Aldrich Co., St. Louis, MO), and fungizone (0.1%, VWR, Radnor, PA) were used

as received to create cell culture media. Two FCC devices, 6x10 size, were submerged in 10 mL of cell culture media held at 37 °C for 72 hours while under agitation.

3T3 fibroblasts (ATCC, Manassas, VA) were seeded in tissue culture plates at a concentration of 5,000 cells per well and placed in a humidified incubator at 37 °C with 5% carbon dioxide (CO_2) for 24 hours. An Eclipse TE 2000-S inverted microscope (Nikon Instruments Inc., Tokyo, Japan) was used to observe cell morphology and confirm even cell distribution. Cell culture media was aspirated and cells were incubated with 100%, 50%, 25%, and 10% extract to assess cytocompatibility. Diluted extracts were prepared by adding fresh cell culture media of the appropriate volume. A cytotoxic control (50% IPA), a cytocompatible control (cell culture media that underwent the extraction process with no device), and an untreated control (fresh cell culture media) were included to ensure the validity of the assay. Cells were incubated at 37 °C with 5% CO_2 for 48 hours.

Extract media was removed, and a neutral red uptake assay (TOX4, Sigma-Aldrich Co., St. Louis, MO) was added to assess cell viability. Neutral red is actively transported across the cell membrane where it accumulates within lysosomes. Cells were incubated with neutral red for 2.5 hours and then fixed using a solution of 0.1% calcium chloride ($CaCl_2$, Sigma-Aldrich Co., St. Louis, MO) in 0.5% formaldehyde (0.5%; Sigma-Aldrich Co., St. Louis, MO). The neutral red was solubilized using a solution of 1% acetic acid (Sigma-Aldrich Co., St. Louis, MO) in 50% ethanol (Sigma-Aldrich Co., St. Louis, MO). The optical density at 540 nm (OD_{540}) was measured using an Infinite® M200 Pro plate reader (Tecan Group Ltd., Männedorf, Switzerland) to quantify the remaining neutral red in each well. Cell viability, expressed as a percentage, was calculated using Equation 1,

where test is the FCC device extract group, blank is a well with no cells, and the control is used as a standard for 100% cell viability.

$$Cell\ viability\,(test) = \frac{OD_{540}\,(test)}{OD_{540}\,(negative\ control)}$$

(4.1)

4.2.6 In vitro Aneurysm Model Deployment

Coiling stability and packing density were assessed in an *in vitro* saccular aneurysm model. A saccular aneurysm with a 6.4 mm major diameter, 4.2 mm minor diameter, and 3.9 mm neck diameter on a 3.1 mm diameter parent vessel was designed in SolidWorks software (Dassault Systems, Waltham, MA). The aneurysm and parent vessel model was printed using a Fortus 360mc 3D printer (Stratasys Ltd., Eden Prairie, MN). The model was suspended in acetone vapor to smooth the outer surface and then dried under vacuum. Sylgard 184 polydimethylsiloxane (PDMS) (Dow Corning Corp., Midland, MI) was cast, cured around the model, and the model was dissolved using a heated base bath. The PDMS aneurysm phantom was placed in a flow system, and 1x phosphate buffered saline (PBS) was heated and pumped through the tubing at average flow rate of 66 ± 2 mL/min. Flow rate was calculated by matching the *in vitro* system Reynold's number to *in vivo* measurements of the middle cerebral artery reported by Reymond et al.[69] Inlet and outlet temperature were maintained at 37 ± 0.5 °C. A 0.022 inch (0.56 mm) ID microcatheter was positioned with the tip in the aneurysm phantom.

FCC devices, 4x6 size, attached to delivery wires were introduced into the microcatheter and advanced to the aneurysm phantom. A device was deployed into the aneurysm until the detachment zone on the delivery wire was out of the microcatheter.

The device was detached by passing a 1.0 mA current through the delivery wire and by placing an uncoated needle in the flow system to electrolytically dissolve the detachment zone on the delivery wire. This was repeated until a subsequent device could not be easily packed into the aneurysm phantom. Bulk packing density, which assumes the foam is a solid volume, was calculated using Equation 2. Material packing density, which accounts for the porosity of the foam, was calculated using Equation 3. Porosity of SMP foam used in these devices was calculated to be 95% using the method published by Hasan et al.[35]

$$Bulk\ packing\ density = \frac{FCC\ bulk\ volume}{Aneurysm\ volume}$$

(4.2)

$$Material\ packing\ density = \frac{Foam\ bulk\ vol \times Foam\ porosity + Coil\ vol}{Aneurysm\ vol}$$

(4.3)

4.2.7 In vivo Aneurysm Model Deployment

Elastase-induced saccular aneurysms were created in New Zealand white rabbits at the origin of the right common carotid artery as reported by Altes et al.[70] Two weeks post aneurysm creation a non-invasive, intra-arterial digital subtraction angiography (DSA) imaging checkup was performed.

At three weeks following aneurysm creation, embolization coil devices were implanted within the aneurysm. A guide catheter was inserted through introducer sheath and positioned in the brachiocephalic artery proximal to the aneurysm. A Rebar-18 microcatheter (ev3 Neurovascular, Irvine, CA) with a 0.021 inch (0.53 mm) ID was positioned through the guide catheter with the microcatheter tip in the aneurysm. An intra-arterial DSA was performed, fluoroscopic images were taken, and the aneurysm and neck diameters were measured. A coil device was introduced into the microcatheter and

deployed under fluoroscopic guidance into the aneurysm until the detachment section was visibly out of the microcatheter. The coil device was then detached in the aneurysm. This was repeated until the aneurysm was sufficiently occluded by angiographic observation, or subsequent devices could not be safely implanted into the aneurysm as directed by the clinician. Following treatment, a DSA was performed. Axium coils, 6x20 size, (ev3 Neurovascular, Irvine, CA) and FCC devices, 2x2 and 4x6 sizes, were used in this study. Device performance was observed and evaluated throughout the procedure. Furthermore, bulk packing density was calculated using Equation 4.2, which assumes the coil devices are solid volumes. Following aneurysm treatment, the sheath entry site is closed, and the animal is returned to the recovery cage.

4.2.8 Explant and Histological Analysis

Histological analysis was performed on the aneurysm sites. Following a 30-day wait period after treatment, a DSA was performed. After angiography, the animal was euthanized using a lethal injection of pentobarbital. The aortic arch and proximal great vessels are exposed and dissected free from surrounding tissues. The aneurysm and parent artery were removed. The specimen was immediately rinsed with normal saline and placed in 10% neutral buffered formalin. The aneurysms were embedded, sectioned, and surface stained using hematoxylin and eosin (H&E) as previously reported by Ding et al.[17] The following features were studied: (1) fibrinous or cellular tissue across the neck, (2) microcompaction at the aneurysm-parent artery interface, (3) tissue reaction around the implant material, and (4) inflammation.

4.3 Results and Discussion

4.3.1 Shape Recovery

SMP foam expansion of foam-coated coil devices in RO water at 37 °C is shown in Figure 3. Three samples were tested. FCC devices expanded to an average diameter of 0.5 mm at 5 min, 0.56 mm at 10 min, and 0.68 mm at 30 min submersion time. The device expansion is slow in physiological conditions, suggesting an estimated working time of 10 min. This estimated working time was confirmed during working time testing discussed in section 3.3. Furthermore, the expansion at 30 min is approximately equivalent to expanded diameters of hydrogel-coated coils published in 2007, though current commercial hydrogel coated devices exhibit decreased expanded diameter in comparison.[52]
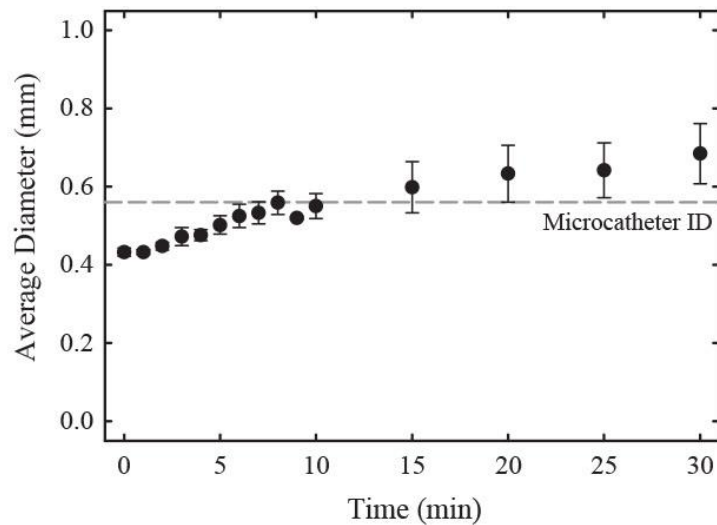
Figure 4.3: SMP foam shape recovery. Average diameter and standard deviation of three FCC devices are shown over time submerged in 37 °C RO water. The dashed line represents the inner diameter (ID) of the microcatheter used in subsequent tests.

4.3.2 Microcatheter Tip Deflection

Tip deflection angle during device deployment is shown in Figure 4 for FCC and GDC-18 2D control devices. Five FCC samples and three control samples were tested. Average peak deflection angle was 3.976 ± 1.58 ° for FCC devices and -2.92 ± 1.51 deg for control devices. Both FCC and control devices exhibited negative tip deflection during deployment of the leading coil loop. However, as the foam-coated section of the FCC passed through the microcatheter bend, the microcatheter tip angle was increased. This contrasts with the control devices, which exhibited minimal change in deflection angle during deployment of the device. This test indicates that FCC devices exhibit greater stiffness than control devices. However, the absolute peak angle of tip deflection of FCC devices is similar to control devices, and the effect of the observed deflection angles on clinical procedures requires additional study. Future studies should investigate alternative stiffness evaluation methods in order to provide comprehensive assessment of FCC device deployment.
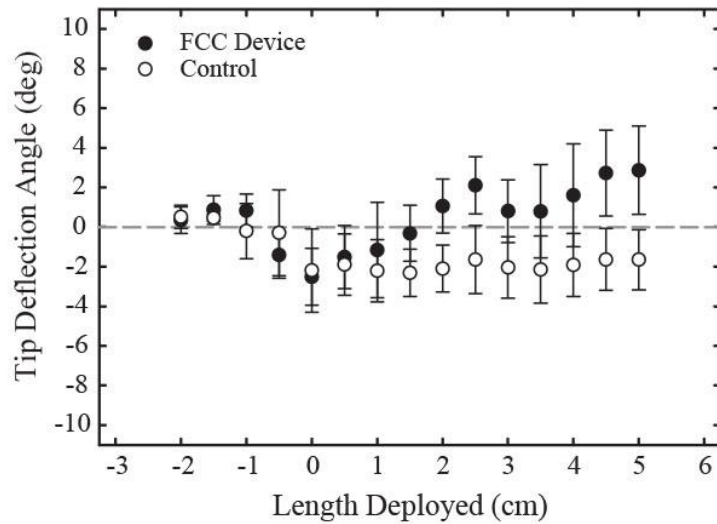
Figure 4.4: Microcatheter tip deflection during device deployment. Average angle of deflection and standard deviation are shown for five FCC and three control devices. Length deployed indicates the length of device deployed out of the microcatheter tip.

4.3.3 Ease of Delivery and Working Time

Delivery forces during advancement through the tortuous pathway are shown in Figure 5 for FCC and GDC-18 2D control devices. Five FCC samples and three control samples were tested. The average peak force was 0.14 ± 0.01 N for FCC devices and 0.18 ± 0.02 N for control devices. One FCC sample delivery force data was omitted for the initial 2.3 cm of travel distance shown in Figure 6 due to excessive resistance exerted on the delivery wire by the hemostasis valve at the microcatheter hub. The valve was opened to decrease resistance at 2.3 cm travel distance, and the remaining dataset includes the complete FCC sample data. No other samples experienced this test error. FCC devices exhibited similar delivery forces as the control devices throughout the travel distance,

72

indicating that the FCC implant provides no additional resistance to delivery through tortuous pathways compared to current commercial devices.
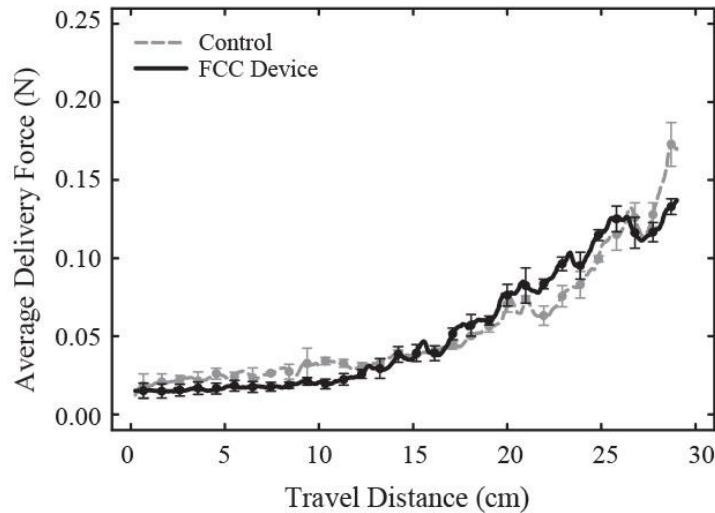
Figure 4.5: Ease of delivery through tortuous pathway. Average delivery force is shown over the travel distance through the tortuous pathway for five FCC devices and three control devices. Standard deviations are shown every 0.9 cm of travel distance. A moving average over 2 mm travel distance was applied to the delivery force data.

Delivery forces during repositioning cycles are shown in Figure 4.5. Five FCC devices were tested. Average absolute peak force was 0.62 ± 0.24 N during deployment and 0.42 ± 0.06 N during retraction. All devices exhibited a working time equal to or greater than 10 min whereby all devices could be fully retracted into the microcatheter after 10 min of total submersion time in simulated physiological conditions. However, samples $3 - 5$ exhibited delivery wire buckling during deployment. During delivery wire buckling, the FCC implants were not deployed out of the microcatheter and thus were not

retracted into the microcatheter during the following cycle. Instead, the buckled delivery wire exerted a negative, or compressive, force on the load cell as indicated by the black arrows in Figure 4.6. At the start of the subsequent deploy cycle, the delivery wire was guided by hand into the microcatheter to prevent buckling. All devices successfully retracted into the microcatheter during the final test cycle.
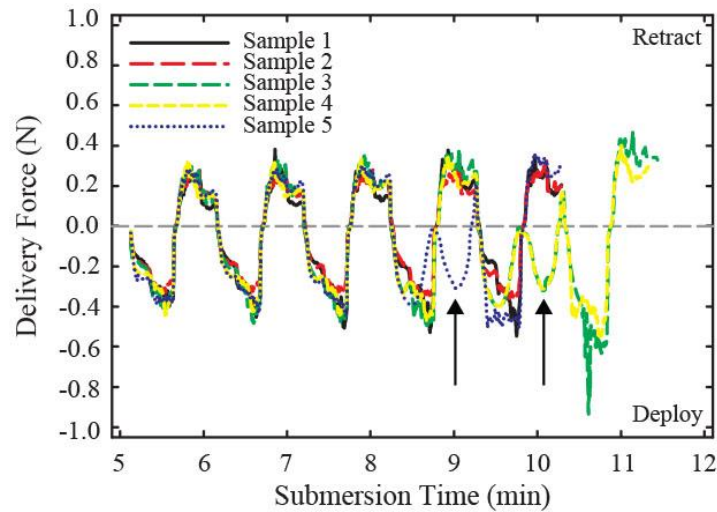
Figure 4.6: Delivery forces during working time assessment. Delivery force for five FCC devices is shown over the submersion time as samples were deployed out and retracted into the microcatheter. Positive force indicates retraction, and negative force indicates deployment. The black arrows indicate that buckling of the delivery wire proximal to the microcatheter hub had occurred on the previous deploy cycle, causing no implant motion and no subsequent retraction on the indicated cycle. A moving average over 0.5 s submersion time was applied to the delivery force data.

FCC devices provide repositioning with minimal to moderate resistance up to and greater than 10 min following introduction of the device into the microcatheter. This working time is greater than the published repositioning time of 5 min for hydrogel coated

74

coils.[27] Working time is a critical metric for clinical adoption as coils must be able to be easily repositioned inside the aneurysm for effective packing and reduced risk of device migration into the parent vessel. Though all FCC devices in this study exhibited working time equal to or greater than 10 min, future studies should investigate greater time points with greater sample sizes to ensure consistent and reliable repositioning during clinically relevant working times.

4.3.4 Cytocompatibility

Cell viability of 3T3 fibroblasts exposed to FCC device extracts is shown in Figure 4.7. Average values are shown for each of 100%, 50%, 25%, and 10% extract concentrations, with six wells per concentration. No morphological changes were observed after cell exposure to device extracts. Average cell viability from device extracts ranged 105-114%. All samples resulting in cell viability greater than 100% show excellent cytocompatibility of FCC devices and provide promise for overall device biocompatibility. Future studies should assess biocompatibility through other standard test methods as cytocompatibility is limited to assessment of extracts and not implanted devices.
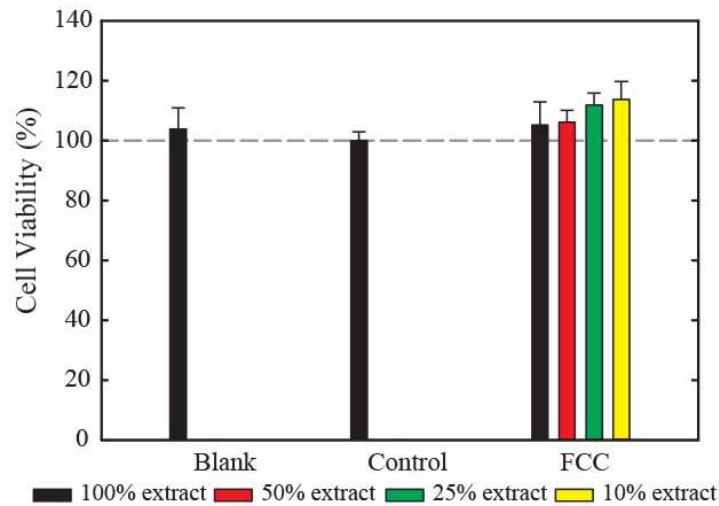
Figure 4.7: Cytocompatibility of FCC devices by neutral red uptake assay. Cell viability of 3T3 fibroblasts is shown for FCC devices compared to blank and control groups. Average viability of six wells is shown with standard deviation for each extract concentration.

4.3.5 In vitro Aneurysm Model Deployment

Device deployment into the *in vitro* aneurysm model is shown in Figure 10. Three FCC devices, 4x6 size, were implanted into the aneurysm model. Packing of the third FCC device was hindered by excessive resistance to buckling. As the aneurysm was packed, less volume was available for coiling to occur, and microcatheter kick-back, i.e. pushing back of the microcatheter tip out of the aneurysm, occurred repeatedly. Although all three devices were successfully implanted into the aneurysm, future studies should investigate buckling force of FCC devices in various sized aneurysm models.
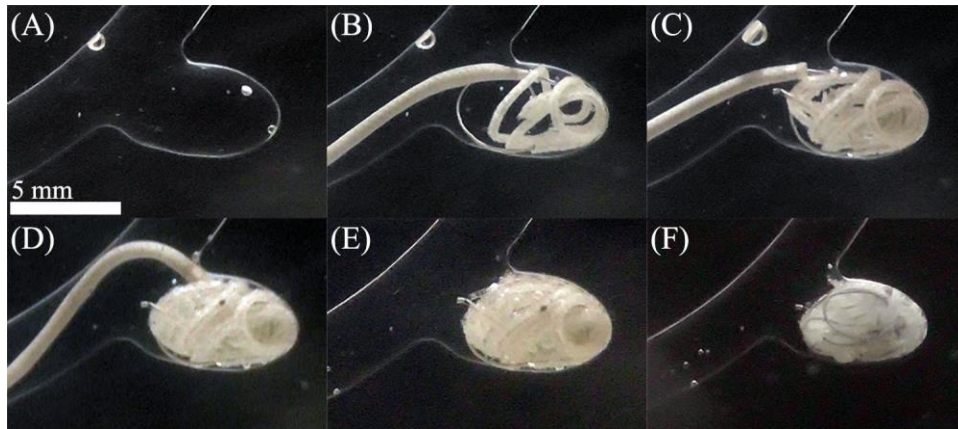
Figure 4.8: FCC device deployment into *in vitro* aneurysm model. (A) Aneurysm model prior to device deployment. Air bubbles in the system are visible. (B) First FCC device deployment. (C) Second FCC device deployment. (D) Third FCC device deployment. (E) Packed aneurysm model 30 min after implant of the third device. (F) Reverse side of packed aneurysm model 30 min after implant of third device.

Bulk packing density was calculated to be 37% with no foam expansion and 92% with foam expansion. These packing densities are similar to published average values for bare platinum coils (30-31%) and hydrogel-coated coils (76-85%).[17,18] As increased packing density has been associated with stable long-term occlusion, the large bulk packing densities achieved with expanded FCC devices suggest that stable long-term occlusion *in vivo* can be achieved.[14,15] However, though FCC device bulk packing density is very similar to current commercial devices, the actual implanted material volume is much less due to the SMP foam porosity. Material packing density was calculated to be 11% for FCC devices in the *in vitro* aneurysm model. This large bulk packing density with small material packing density is potentially advantageous as the FCC device provides scaffolding throughout the majority of the aneurysm space while allowing the majority of the volume to be filled by stable thrombus formation and healed tissue. This may improve

upon previous devices as bare platinum coils provide less bulk occlusion, and hydrogel-coated coils displace blood instead of providing porous scaffolding throughout the aneurysm volume. *In vivo* studies should be conducted to investigate the effect of high porosity occlusion from FCC devices on aneurysm treatment.

4.3.6 In vivo Aneurysm Model Treatment

FCC devices were successfully delivered and implanted into three aneurysms with minimal procedural complications. Once the devices were clear of the delivery sheath, they delivered smoothly through the microcatheter with minimal resistance. However, during deployment and packing, devices exhibited excessive stiffness and caused significant microcatheter kick-back, similar to that observed during *in vitro* aneurysm deployment. As shown in Figure 4.9, the device stiffness resulted in visibly sparse packing of the FCC devices into the aneurysm and one case of a single coil loop implanted in the parent artery. Aneurysm volume, devices implanted, and bulk packing density are listed for each aneurysm in Table 4.1. Average bulk packing density was calculated to be 51.6 ± 3.1%, which is greater than published values for bare platinum coils (30-31%).[17,18] This suggests that positioning the implants localized to the aneurysm dome may have resulted in increased occlusion density within the bulk implanted mass compared to bare platinum coils. This increased packing density is hypothesized to increase thrombus stability and healing within the bulk implanted mass. Thus, if packing and positioning of FCC devices can be improved and leave less untreated aneurysm volume, the resulting bulk implanted mass may provide improved healing and long-term stability compare to bare platinum coils. FCC devices exhibited less visibility under fluoroscopy compared to the Axium coil

used, though this is expected as the OD of the platinum coil used in FCC devices is less than the OD of the Axium coil. FCC devices were not able to be tracked in the guide catheter and were difficult to track while in the microcatheter. These limitations of excessive stiffness and insufficient radiopacity must be addressed prior to translation to clinical use. However, all devices were successfully detached and post-treatment angiography showed minimal contrast infiltration into the aneurysm dome with contrast infiltration into the neck of all aneurysms. The minimal contrast infiltration into the sparsely packed aneurysm domes suggests thrombus formation within the porous SMP foam during the procedure.
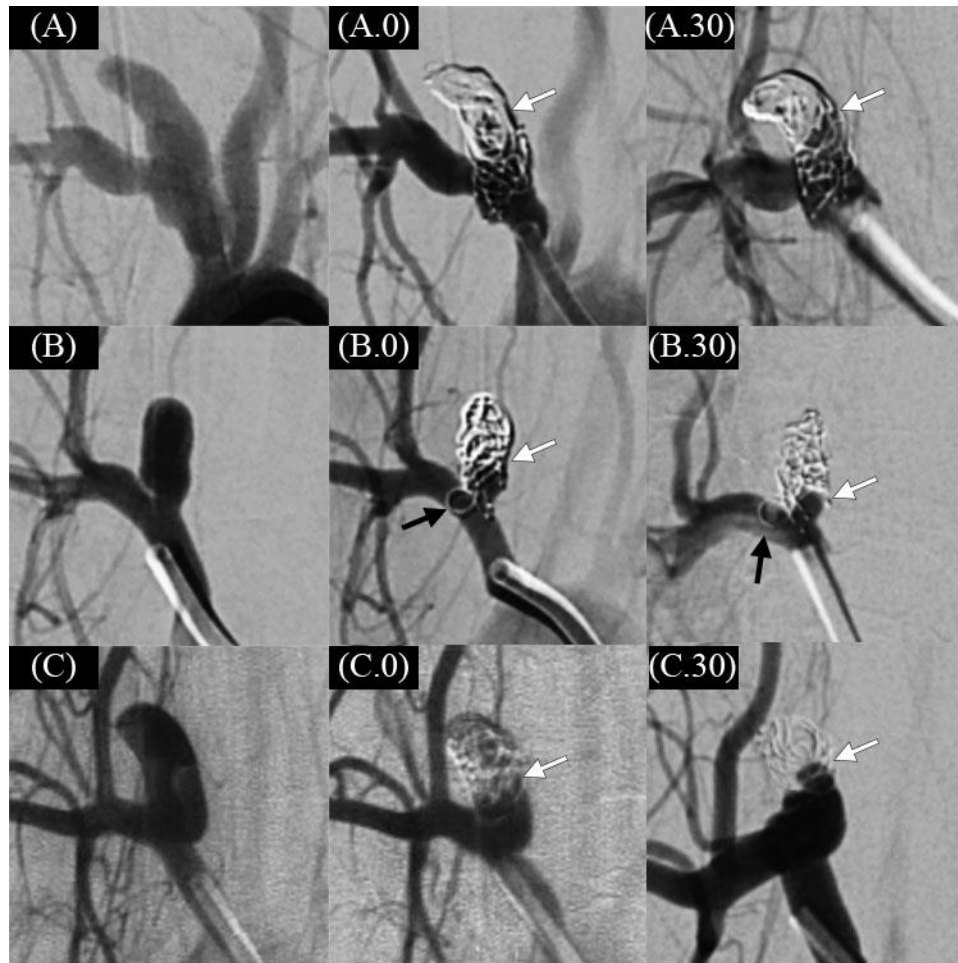
Figure 4.9: Digital subtraction angiography (DSA) images of the aneurysms prior to and after treatment. The top row shows DSA images of aneurysm A prior to treatment (A), after treatment (A.0), and 30 days after treatment (A.30), where white arrows indicate the edge of contrast infiltration through the neck and into the dome of the aneurysm. The middle row shows DSA images of aneurysm B prior to treatment (B), after treatment (B.0), and 30 days after treatment (B.30), where white arrows indicate the edge of contrast infiltration through the neck and into the dome of the aneurysm and black arrows indicate a section of an implanted device left in the parent artery after premature detachment occurred. The bottom row shows DSA images of aneurysm C prior to treatment (C), after treatment (C.0), and 30 days after treatment (C.30), where white arrows indicate the edge of contrast infiltration through the neck and into the dome of the aneurysm.

Table 4.1: *In vivo* Aneurysm Sizes, Packing Density

Aneurysm ID	Aneurysm volume (mm³)	Implanted Devices	Bulk Packing Density
A	87	1 Axium6x20 1 FCC4x6 2 FCC2x2	53%
B	76	1 FCC4x6 4 FCC2x2	55%
C	90	2 FCC4x6 2 FCC2x2	48%

4.3.7 Histological Analysis

Explanted aneurysms displayed significant neck remnants with loose connective tissue filling the majority of aneurysms in and around the implanted devices. Gross evaluation of each aneurysm showed neck remnants open to the parent artery as also visible in 30 day DSA images. A thin membrane coats the surface of the implant materials, indicating partial to nearly complete endothelial layer development. Figure 4.10 shows sectioned slide images of each aneurysm evaluated during histological analysis. Connective tissue with dense, diffuse inflammatory tissue is visible within and around the eosinophilic SMP foam material. Multinucleated giant cells were primarily surrounding the SMP foam material with some lymphocytes and macrophages distributed throughout the tissue. A nearly complete endothelial layer with thin and thick neointima lined the interface between the connective tissue and neck remnant the aneurysms. Poorly organized thrombus is visible at the neck remnant interface in aneurysms A and C. Furthermore, the neointima and thrombus layers present in aneurysms A and C appear concave, indicating some implant compaction.
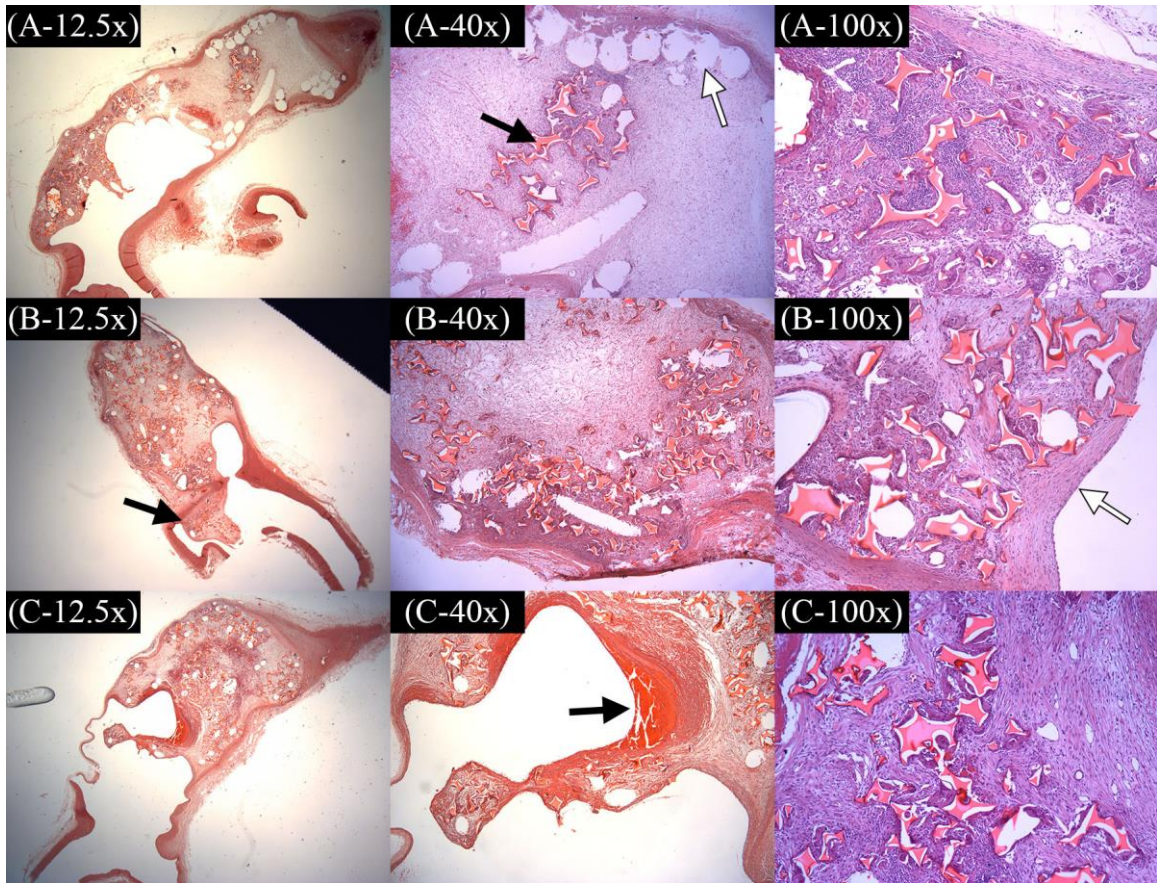
Figure 4.10: Images of H&E stained and sectioned slides from histological analysis at various magnification. The top row shows slide images of aneurysm A at 12.5x (A-12.5x), 40x (A-40x), and 100x (A-100x) magnification. The black arrow indicates the eosinophilic SMP foam material, and the white arrow indicates where the Axium coil was positioned, though the coil was removed during sectioning. The middle row shows slide images of aneurysm B at 12.5x (B-12.5x), 40x (B-40x), and 100x (B-100x) magnification. The black arrow indicates the connective tissue within and surrounding the coil within the parent artery, and the white arrow indicates the endothelial and neointima layer at the interface between the connective tissue in the dome and the neck remnant. The bottom row shows slide images of aneurysm C at 12.5x (C-12.5x), 40x (C-40x), and 100x (C-100x) magnification. The black arrow indicates the poorly organized thrombus present at the interface between the connective tissue in the dome and the neck remnant.

Despite the poor packing of the aneurysms, the histological analysis showed

cellular infiltration and tissue healing within and around the implanted devices that are

very promising for achieving stable aneurysm treatment. The desired healing process for aneurysm treatment includes thrombus formation with stable fibrin mesh development, unextended acute inflammation, T-helper cell guided recruitment of macrophages to break down fibrin, and the recruitment of fibroblasts to produce collagen to form granulation tissue.[71] This healing process progresses from the outer shell of the aneurysm and into the central core of the aneurysm. Furthermore, development of a neointima layer across the aneurysm neck is also desired to prevent recanalization. The 30-day treated aneurysms exhibited dense connective tissue within the outer zone of the aneurysm and loose connective tissue within the center of the occluded volumes. The loose connective tissue formation within the gaps between implanted materials, as shown in Figure 4.10 (B-40x), demonstrates near complete resolution of the fibrin mesh and early formation of collagenous tissue. Use of phosphotungstic acid haematoxylin (PTAH) and Masson's trichrome stains in future studies may allow for qualitative and quantitative analysis of the residual fibrin and deposited collagen. All aneurysms showed an inflammation response led by macrophage activity, primarily in the form of multinucleated giant cells. The recruitment of macrophages is a critical component of the healing process, as T-helper cells and macrophages can signal an undesired chronic inflammation response or can signal continued healing by breaking down fibrin and recruiting fibroblasts. The development of loose and dense connective tissues as well as the stable formation of multinucleated giant cells around the implanted material indicate that T-helper cells are guiding the cellular response towards injury resolution and granulation tissue formation, as opposed to the undesired chronic inflammation response. Additionally, the neointima

83

layer formation at the interface between the connective tissue within and around the implanted material and the neck remnant is also promising, as this suggests that packing of the SMP foam material at or near the aneurysm neck would result in a stable neointima formation across the neck. The unorganized thrombus formation can be attributed to hemodynamics and recirculation zones expected from the uneven surface of the implanted mass. The unorganized thrombus would be expected to be resolved with improved packing and prevention of neck remnants. Overall, the inflammation response within the explanted aneurysms is very promising and suggests the implant materials have prompted the desired healing response; however, longer time-point implants, such as 90-day implants, will be required to confirm that the healing process progresses as desired beyond the currently tested time-point.

4.4 Conclusions

A shape memory polymer (SMP) foam-coated coil (FCC) embolization device was designed and demonstrates effective delivery and packing performance for treatment of intracranial saccular aneurysms. The FCC device provides clinician-familiar deliverability and use combined with great packing volume and scaffolding capability of porous SMP foam. Excellent cytocompatibility is a promising early result in showing biocompatibility, though several more tests are required to continue assessment of biocompatibility. FCC devices exhibited smooth delivery, but difficult packing in both benchtop and rabbit elastase aneurysm models highlights the need to improving device stiffness. However, though packing in rabbit aneurysms was poor, the tissue response suggests a desired healing process and a promising indication that the more effectively packed FCC devices

will prompt stable, long-term tissue healing. Overall, this work demonstrates good promise for clinical realization of the SMP foam-coated coil embolization device for treatment of intracranial saccular aneurysms.

CHAPTER V

CONCLUSIONS

5.1 Summary

A shape memory polymer (SMP) foam-coated coil (FCC) neurovascular embolization device was designed and developed for treatment of intracranial saccular aneurysms. The SMP foam material and device prototypes were characterized and tested using various *in vitro* and *in vivo* models to evaluate performance and achieve design goals of a clinically feasible device. The resulting FCC device provides clinician-familiar deliverability and use combined with the large packing volume and tissue scaffolding capability of porous SMP foam.

Solvent-stimulated SMP foam actuation was investigated as a means of achieving working time greater than the clinical requirement with the ability to expand the SMP foam on demand. Actuation of hydrophobic SMP foams using DMSO and EtOH was shown to be an effective alternative shape memory trigger to direct heating. Dramatic decreases in T_g were observed with exposure to water, DMSO, and EtOH. EtOH was shown to decrease SMP foam relaxation times to less than 1 min in DMA kinetic experiments. Furthermore, rapid shape recovery and volume swelling were observed for SMP foams in high concentrations of both DMSO and EtOH, as well as in decreased concentrations of EtOH. This work demonstrated that both DMSO and EtOH are effective at triggering actuation of SMP foams, including in aqueous environments, and that solvent selection is critical to the effectiveness of this actuation technique.

A SMP foam-over-wire (FOW) neurovascular embolization device was evaluated using *in vitro* and *in vivo* saccular aneurysm models as an initial prototype design for a clinically feasible neurovascular embolization device that implements the advantages of SMP foams. FOW devices demonstrated effective delivery and stable implantation *in vitro*. *In vivo* porcine aneurysms were successfully occluded using FOW devices with theoretical volume occlusion values greater than 72% and rapid, stable thrombus formation. FOW devices were successful in treating sidewall aneurysm models, though the study suggested a need to improve the deliverability and radiopacity of the devices and to evaluate the occlusion effectiveness in more clinically relevant aneurysm geometries.

A SMP foam-coated coil (FCC) embolization device was designed and demonstrates effective delivery and repositioning performance for treatment of intracranial saccular aneurysms. The FCC device provides clinician-familiar deliverability and use combined with large packing density and scaffolding capability of porous SMP foam. Excellent cytocompatibility is a promising early result in showing biocompatibility, though several more tests are required to continue assessment of biocompatibility. FCC devices exhibited smooth delivery, but difficult packing in both benchtop and rabbit elastase aneurysm models highlights the need to improving device stiffness. However, though packing in rabbit aneurysms was poor, the tissue response suggests a desired healing process and a promising indication that the more effectively packed FCC devices will prompt stable, long-term tissue healing. Overall, this work demonstrates good promise for clinical realization of the SMP foam-coated coil embolization device for treatment of intracranial saccular aneurysms.

5.2 Significance of Work

Aneurysmal subarachnoid hemorrhage (aSAH), caused by ruptured intracranial aneurysms, results in high morbidity and mortality rates. At least 25% of patients die due to aSAH, and approximately 50% of survivors are left with persistent neurological deficit.[4] Standard endovascular treatment of implanting embolization coil devices into saccular aneurysms has been shown to be an effective treatment method, but it remains marked by aneurysm recanalization or recurrence despite continued development of new device technologies.[12,13] Aneurysm recurrence or recanalization refer to the return of blood flow into an occluded aneurysm and increased risk of rupture and hemorrhage. Early studies of bare platinum coils reported recurrence in 21 – 34% of cases.[20,21] Based on these recurrence rates, polymer-embedded coils were developed with the intent to improve healing and reduce recanalization rates. However, new coil technologies have not improved recurrence rates, and clinical recurrence remains a primary limitation of endovascular coiling, overall occurring in 21% of cases and requiring retreatment in 10% of cases.[12]

Polyurethane-based shape memory polymer (SMP) foams are advantageous biomaterials for endovascular embolization applications due to their shape recovery capability and interconnected, large surface area porosity.[1,31,32] SMP foams exhibit promising cytocompatibility, increased implanted angiographic occlusion, integrated connective tissue post-implant, and a thicker neointima layer compared to bare platinum coils in porcine saccular aneurysm models.[1,31,33] However, previously developed devices utilizing SMP foam for neurovascular embolization treatment were limited by required

catheter sizes, insufficient flexibility and radiopacity, and inconsistent device stability within the aneurysm sac.[32]

In chapter II, solvent-stimulated SMP foam actuation was demonstrated as a means of achieving working time greater than the clinical requirement with the ability to expand the SMP foam on demand. Actuation of hydrophobic SMP foams using DMSO and EtOH was shown to be an effective alternative shape memory trigger to direct heating. This work was useful in characterizing and improving the expansion behavior of the SMP foams for embolization coil application. Though EtOH and DMSO are not ideal solvents for neurovascular applications due to moderate to severe toxicological effects, this work serves as a proof of concept of SMP foam actuation control using non-water solvents and provides insight into mechanisms that can be investigated for future material and device design work.[46,47] Overall, this work demonstrates great potential for use of solvents as an alternative actuation stimulant for polyurethane-based SMP foams and may improve feasibility of using SMP materials in a variety of applications.

In chapter III, a SMP foam-over-wire (FOW) neurovascular embolization device demonstrated promising performance in *in vitro* and *in vivo* environments as an initial prototype design for a clinically feasible neurovascular embolization device. The FOW design implemented the SMP foams in a microcatheter-compatible geometry to achieve greater volume occlusion than current commercial devices. This device was improved upon as discussed in chapter IV, where a SMP foam-coated coil (FCC) embolization device demonstrated effective delivery, large packing density, and excellent cytocompatibility. Though packing into rabbit aneurysms was difficult, the tissue response

suggests a desired healing process and a promising indication that the more effectively packed FCC devices will prompt stable, long-term tissue healing.

Overall, the device designed through this work demonstrates excellent potential for improving long-term clinical outcomes for patients with intracranial saccular aneurysms, whether ruptured or unruptured. The FFC device enables clinician-familiar deliverability that results in implantation of the SMP foam in order to utilize its large volume occlusion and improved tissue response, which are promising improvements over current commercial devices. This device has the potential to dramatically decrease clinical recanalization and recurrence rates, which will reduce the costs and risks associated with retreatment or re-rupture, ultimately improving patient outcomes.

5.3 Challenges and Future Directions

The SMP foam-coated coil device is a promising candidate for clinical application in treatment of intracranial saccular aneurysms. Although the device has demonstrated excellent capabilities and properties necessary to meet the needs of the clinician and patient, further improvements are required to improve clinical adoption and reduce risks of procedural complications. Furthermore, although the characterization and testing performed in this work lays a foundation for the device development, more rigorous benchtop and animal testing, including within ISO 10993 guidelines, will be required to demonstrate device safety and efficacy for clinical application. Additionally, the solvent-stimulated actuation methodology exhibited promising results, particularly for non-neurovascular applications, but development of new materials is necessary to allow application in the neurovascular environment.

Future development of the solvent-stimulated actuation method should focus on material design and synthesis that respond to exposure to less toxic substances compared to DMSO or EtOH. Perfluorocarbon materials, such as perflourodecalin, perflourophenanthrene, or perflouro-n-hexane, have been researched for artificial blood applications and therefore are the most desirable for vascular applications as the risks associated with injecting these materials are low. Development of a shape memory material capable of rapid, controlled actuation in the presence of perfluorocarbons could provide complete clinician control over the SMP actuation compared to the current method of tailoring the expansion profile with exposure to physiological environments. This development would also expand the capabilities of this method into other fields and improve overall understanding of the mechanisms of shape memory materials.

Future development of the FCC device should focus on increasing the device flexibility, packing performance, and radiopacity without unduly sacrificing the volume occlusion and healing properties of the SMP foam. The current FCC devices demonstrated excellent potential in tracking through neurovascular tortuosity and minimal microcatheter tip deflection; however, packing the foam-coated coil into small volumes requires excessive force and increased risk of vessel perforation, coil migration, or other complications. Device flexibility and radiopacity could be improved by decreasing the volume of foam coating as well as increasing the coil volume. The SMP foam in its compressed state is a stiff material, as a result of achieving the slowed expansion profile required for ample clinician working time. Thus, by reducing the overall volume of the SMP foam on the coil, the overall stiffness of the device could be improved. However,

this will have to be carefully tailored against over performance characteristics, primarily working time and packing density. The increase in coil volume is a simple solution for improving the fluoroscopic visualization of the device, though this will also have to be characterized to ensure that the mechanical stability of the SMP foam on the coil is not decreased.

REFERENCES

1. Rodriguez JN, Clubb FJ, Wilson TS, Miller MW, Fossum TW, *et al.* In vivo response to an implanted shape memory polyurethane foam in a porcine aneurysm model. Journal of Biomedical Materials Research Part A 2014;102(5):1231-1242.

2. Carter BS, Sheth S, Chang E, Sethl M, Ogilvy CS. Epidemiology of the size distribution of intracranial bifurcation aneurysms: smaller size of distal aneurysms and increasing size of unruptured aneurysms with age. Neurosurgery 2006;58(2):217-223.

3. Humphrey JD. Cardiovascular solid mechanics: cells, tissues, and organs. New York: Springer; 2002.

4. Connolly ES, Rabinstein AA, Carhuapoma JR, Derdeyn CP, Dion J, *et al.* Guidelines for the management of aneurysmal subarachnoid hemorrhage: A guideline for healthcare professionals from the American Heart Association/American Stroke Association. Stroke 2012;43(6):1711-1737.

5. Carod-Artal FJ, Egido JA. Quality of life after stroke: The importance of a good recovery. Cerebrovascular Diseases 2009;27(Suppl. 1):204-214.

6. Rinne J, Hernesniemi J, Puranen M, Saari T. Multiple intracranial aneurysms in a defined population: prospective angiographic and clinical study. Neurosurgery 1994;35(5):803-808.

7. Brinjikji W, Kallmes DF, Kadirvel R. Mechanisms of healing in coiled intracranial aneurysms: A review of the literature. American Journal of Neuroradiology 2015;36(7):1216-1222.

8. Guglielmi G, Vinuela F, Sepetka I, Macellari V. Electrothrombosis of saccular aneurysms via endovascular approach 1. Electrochemical basis, technique, and experimental results. Journal of Neurosurgery 1991;75(1):1-7.

9. Guglielmi G, Vinuela F, Dion J, Duckwiler G. Electrothrombosis of saccular aneurysms via endovascular approach 2. Preliminary clinical experience. Journal of Neurosurgery 1991;75(1):8-14.

10. White JB, Ken CGM, Cloft HJ, Kallmes DF. Coils in a nutshell: A review of coil physical properties. American Journal of Neuroradiology 2008;29(7):1242-1246.

11. Murayama Y, Vinuela F, Tateshima S, Song JK, Gonzalez NR, *et al.* Bioabsorbable polymeric material coils for embolization of intracranial

aneurysms: a preliminary experimental study. Journal of Neurosurgery 2001;94(3):454-463.

12.   Ferns SP, Sprengers MES, van Rooij WJ, Rinkel GJE, van Rijn JC*, et al.* Coiling of intracranial aneurysms: A systematic review on initial occlusion and reopening and retreatment rates. Stroke 2009;40(8):523-529.

13.   Molyneux AJ, Kerr RSC, Yu LM, Clarke M, Sneade M*, et al.* International subarachnoid aneurysm trial (ISAT) of neurosurgical clipping versus endovascular coiling in 2143 patients with ruptured intracranial aneurysms: a randomised comparison of effects on survival, dependency, seizures, rebleeding, subgroups, and aneurysm occlusion. Lancet 2005;366(9488):809-817.

14.   Knap D, Gruszczyńska K, Partyka R, Ptak D, Korzekwa M*, et al.* Results of endovascular treatment of aneurysms depending on their size, volume and coil packing density. Neurologia i Neurochirurgia Polska 2013;47(5):467-475.

15.   Leng B, Zheng Y, Ren J, Xu Q, Tian Y*, et al.* Endovascular treatment of intracranial aneurysms with detachable coils: correlation between aneurysm volume, packing, and angiographic recurrence. Journal of NeuroInterventional Surgery 2014;6(8):595-599.

16.   Yuki I, Lee D, Murayama Y, Chiang A, Vinters HV*, et al.* Thrombus organization and healing in an experimental aneurysm model part II. The effect of various types of bioactive bioabsorbable polymeric coils. Journal of Neurosurgery 2007;107(1):109-120.

17.   Ding YH, Dai DY, Lewis DA, Cloft HJ, Kallmes DF. Angiographic and histologic analysis of experimental aneurysms embolized with platinum coils, Matrix, and HydroCoil. American Journal of Neuroradiology 2005;26(7):1757-1763.

18.   Gaba RC, Ansari SA, Roy SS, Marden FA, Viana MA*, et al.* Embolization of intracranial aneurysms with hydrogel-coated coils versus inert platinum coils: effects on packing density, coil length and quantity, procedure performance, cost, length of hospital stay, and durability of therapy. Stroke 2006;37(6):1443-1450.

19.   Szikora I, Seifert P, Hanzely Z, Kulcsar Z, Berentei Z*, et al.* Histopathologic evaluation of aneurysms treated with Guglielmi detachable coils or Matrix detachable microcoils. American Journal of Neuroradiology 2006;27(2):283-288.

20.   Murayama Y, Nien YL, Duckwiler G, Gobin YP, Jahan R*, et al.* Guglielmi detachable coil embolization of cerebral aneurysms: 11 years' experience. Journal of Neurosurgery 2003;98(5):959-966.

21.   Raymond J, Guilbert F, Weill A, Georganos SA, Juravsky L*, et al.* Long-term angiographic recurrences after selective endovascular treatment of aneurysms with detachable coils. Stroke 2003;34(6):1398-1403.

22.   Bendszus M, Solymosi L. Cerecyte coils in the treatment of intracranial aneurysms: A preliminary clinical study. American Journal of Neuroradiology 2006;27(10):2053-2057.

23.   McDougall CG, Johnston SC, Gholkar A, Barnwell SL, Vazquez Suarez JC*, et al.* Bioactive versus bare platinum coils in the treatment of intracranial aneurysms: The MAPS (matrix and platinum science) trial. American Journal of Neuroradiology 2014;35(5):935-942.

24.   Fiorella D, Albuquerque FC, McDougall CG. Durability of aneurysm embolization with Matrix detachable coils. Neurosurgery 2006;58(1):51-58.

25.   Niimi Y, Song J, Madrid M, Berenstein A. Endosaccular treatment of intracranial aneurysms using Matrix coils - Early experience and midterm follow-up. Stroke 2006;37(4):1028-1032.

26.   Molyneux AJ, Clarke A, Sneade M, Mehta Z, Coley S*, et al.* Cerecyte coil trial: angiographic outcomes of a prospective randomized trial comparing endovascular coiling of cerebral aneurysms with either Cerecyte or bare platinum coils. Stroke 2012;43(10):2544-2550.

27.   Cloft HJ, Kallmes DF. Aneurysm packing with HydroCoil embolic system versus platinum coils: initial clinical experience. Amer J Neurorad 2004;25(1):60-62.

28.   White PM, Lewis SC, Gholkar A, Sellar RJ, Nahser H*, et al.* Hydrogel-coated coils versus bare platinum coils for the endovascular treatment of intracranial aneurysms (HELPS): a randomised controlled trial. Lancet 2011;377(9778):1655-1662.

29.   Wilson TS, Bearinger JP, Herberg JL, Marion JE, Wright WJ*, et al.* Shape memory polymers based on uniform aliphatic urethane networks. Journal of Applied Polymer Science 2007;106(1):540-551.

30.   Lendlein A, Kelch S. Shape-memory polymers. Angewandte Chemie-International Edition 2002;41(12):2034-2057.

31.   Horn J, Hwang W, Jessen SL, Keller BK, Miller MW*, et al.* Comparison of shape memory polymer foam versus bare metal coil treatments in an in vivo porcine sidewall aneurysm model. Journal of Biomedical Materials Research Part B: Applied Biomaterials 2016:00:000-000.

32. Hwang W, Singhal P, Miller MW, Maitland DJ. In vitro study of transcatheter delivery of a shape memory polymer foam embolic device for treating cerebral aneurysms. Journal of Medical Devices 2013;7(2):020932-020932.

33. Singhal P, Rodriguez JN, Small W, Eagleston S, Van de Water J*, et al.* Ultra low density and highly crosslinked biocompatible shape memory polyurethane foams. Journal of Polymer Science Part B: Polymer Physics 2012;50(10):724-737.

34. Hasan SM, Raymond JE, Wilson TS, Keller BK, Maitland DJ. Effects of isophorone diisocyanate on the thermal and mechanical properties of shape-memory polyurethane foams. Macromolecular Chemistry and Physics 2014;215(24):2420-2429.

35. Hasan SM, Harmon G, Zhou F, Raymond JE, Gustafson TP*, et al.* Tungsten-loaded SMP foam nanocomposites with inherent radiopacity and tunable thermo-mechanical properties. Polymers for Advanced Technologies 2016;27(2):195-203.

36. Rodriguez JN, Yu YJ, Miller MW, Wilson TS, Hartman J*, et al.* Opacification of shape memory polymer foam designed for treatment of intracranial aneurysms. Annals of Biomedical Engineering 2011;40:883.

37. Weems AC, Raymond JE, Wacker KT, Gustafson TP, Keller B*, et al.* Examination of radio-opacity enhancing additives in shape memory polyurethane foams. Journal of Applied Polymer Science 2015;132(23):42054.

38. Du H, Zhang J. Solvent induced shape recovery of shape memory polymer based on chemically cross-linked poly (vinyl alcohol). Soft Matter 2010;6(14):3370-3376.

39. Yang B, Huang W, Li C, Li L. Effects of moisture on the thermomechanical properties of a polyurethane shape memory polymer. Polymer 2006;47(4):1348-1356.

40. Lv H, Leng J, Liu Y, Du S. Shape-memory polymer in response to solution. Advanced Engineering Materials 2008;10(6):592-595.

41. Singhal P, Boyle A, Brooks ML, Infanger S, Letts S*, et al.* Controlling the actuation rate of low-density shape-memory polymer foams in water. Macromolecular Chemistry and Physics 2013;214(11):1204-1214.

42. Yu YJ, Hearon K, Wilson TS, Maitland DJ. The effect of moisture absorption on the physical properties of polyurethane shape memory polymer foams. Smart Materials and Structures 2011;20(8):085010.

43.   Cekirge HS, Saatci I, Ozturk MH, Cil B, Arat A, *et al.* Late angiographic and clinical follow-up results of 100 consecutive aneurysms treated with Onyx reconstruction: largest single-center experience. Neuroradiology 2006;48(2):113-126.

44.   Murayama Y, Viñuela F, Tateshima S, Viñuela Jr F, Akiba Y. Endovascular treatment of experimental aneurysms by use of a combination of liquid embolic agents and protective devices. American Journal of Neuroradiology 2000;21(9):1726-1735.

45.   Piske RL, Kanashiro LH, Paschoal E, Agner C, Lima SS, *et al.* Evaluation of Onyx HD-500 embolic system in the treatment of 84 wide-neck intracranial aneurysms. Neurosurgery 2009;64(5):865-874.

46.   Sampei K, Hashimoto N, Kazekawa K, Tsukahara T, Iwata H, *et al.* Histological changes in brain tissue and vasculature after intracarotid infusion of organic solvents in rats. Neuroradiology 1996;38(3):291-294.

47.   Hamada J-I, Kai Y, Morioka M, Kazekawa K, Ishimaru Y, *et al.* A nonadhesive liquid embolic agent composed of ethylene vinyl alcohol copolymer and ethanol mixture for the treatment of cerebral arteriovenous malformations: experimental study. Journal of Neurosurgery 2002;97(4):889-895.

48.   Chaloupka JC, Huddle DC, Alderman J, Fink S, Hammond R, *et al.* A reexamination of the angiotoxicity of superselective injection of DMSO in the swine rete embolization model. American Journal of Neuroradiology 1999;20(3):401-410.

49.   Murayama Y, Viñuela F, Ulhoa A, Akiba Y, Ducwiler GR, *et al.* Nonadhesive liquid embolic agent for cerebral arteriovenous malformations: Preliminary histopathological studies in swine rete mirabile. Neurosurgery 1998;43(5):1164-1172.

50.   Reed KW, Yalkowsky SH. Lysis of human red blood cells in the presence of various cosolvents. PDA Journal of Pharmaceutical Science and Technology 1985;39(2):64-69.

51.   Mottu F, Laurent A, Rüfenacht DA, Doelker E. Organic solvents for pharmaceutical parenterals and embolic liquids: A review of toxicity data. PDA Journal of Pharmaceutical Science and Technology 2000;54(6):456-469.

52.   Cruise GM, Shum JC, Plenk H. Hydrogel-coated and platinum coils for intracranial aneurysm embolization compared in three experimental models using

computerized angiographic and histologic morphometry. Journal of Materials Chemistry 2007;17(38):3965-3973.

53.   Duerig T, Pelton A, Stockel D. An overview of nitinol medical applications. Materials Science and Engineering: A – Structural Materials: Properties Microstructure and Processing 1999;273:149-160.

54.   Weber W, Bendszus M, Kis B, Boulanger T, Solymosi L, *et al.* A new self-expanding nitinol stent (Enterprise) for the treatment of wide-necked intracranial aneurysms: initial clinical and angiographic results in 31 aneurysms. Neuroradiology 2007;49(7):555-561.

55.   Hearon K, Singhal P, Horn J, Small W, Olsovsky C, *et al.* Porous shape-memory polymers. Polymer Reviews 2013;53(1):41-75.

56.   Lu H, Huang WM, Fu Y, Leng J. Quantitative separation of the influence of hydrogen bonding of ethanol/water mixture on the shape recovery behavior of polyurethane shape memory polymer. Smart Materials and Structures 2014;23(12):125041.

57.   Kanikkannan N, Kandimalla K, Lamba S, Singh M. Structure-activity relationship of chemical penetration enhancers in transdermal drug delivery. Current Medicinal Chemistry 2000;7(6):593-608.

58.   Rodriguez JN, Miller MW, Boyle A, Horn J, Yang C-K, *et al.* Reticulation of low density shape memory polymer foam with an in vivo demonstration of vascular occlusion. Journal of the Mechanical Behavior of Biomedical Materials 2014;40:102-114.

59.   Lu H. A simulation method to analyze chemo-mechanical behavior of swelling-induced shape-memory polymer in response to solvent. Journal of Applied Polymer Science 2012;123(2):1137-1146.

60.   Slob MJ, van Rooij WJ, Sluzewski M. Influence of coil thickness on packing, re-opening and retreatment of intracranial aneurysms: a comparative study between two types of coils. Neurological Research 2005;27(Supplement-1):116-119.

61.   Wakhloo AK, Gounis MJ, Sandhu JS, Akkawi N, Schenck AE, *et al.* Complex-shaped platinum coils for brain aneurysms: higher packing density, improved biomechanical stability, and midterm angiographic outcome. American Journal of Neuroradiology 2007;28(7):1395-1400.

62.	Sluzewski M, van Rooij WJ, Slob MJ, Bescos JO, Slump CH, *et al.* Relation between aneurysm volume, packing, and compaction in 124 cerebral aneurysms treated with coils. Radiology 2004;231(3):653-658.

63.	Geyik S, Ertugrul O, Yavuz K, Geyik P, Saatci I, *et al.* Comparison of bioactive coils and bare platinum coils for treatment of intracranial aneurysms: a matched-pair analysis. Journal of Neurosurgery 2010;112(4):709-713.

64.	Landsman MLJ, Kwant G, Mook GA, Zijlstra WG. Light-absorbing properties, stability, and spectral stabilization of indocyanine green. Journal of Applied Physiology 1976;40(4):575-583.

65.	Holdsworth D, Norley C, Frayne R, Steinman D, Rutt B. Characterization of common carotid artery blood-flow waveforms in normal human subjects. Physiological Measurement 1999;20(3):219-240.

66.	Guglielmi G, Ji C, Massoud TF, Kurata A, Lownie SP, *et al.* Experimental saccular aneurysms. Neuroradiology 1994;36(7):547-550.

67.	Boyle AJ, Landsman TL, Wierzbicki MA, Nash LD, Hwang W, *et al.* In vitro and in vivo evaluation of a shape memory polymer foam-over-wire embolization device delivered in saccular aneurysm models. Journal of Biomedical Materials Research Part B Applied Biomaterials 2015;00:000-000.

68.	Sugiu K, Martin J-B, Jean B, Gailloud P, Mandai S, *et al.* Artificial cerebral aneurysm model for medical testing, training, and research. Neurologia Medico-chirurgica 2003;43(2):69-73.

69.	Reymond P, Merenda F, Perren F, Rüfenacht D, Stergiopulos N. Validation of a one-dimensional model of the systemic arterial tree. American Journal of Physiology - Heart and Circulatory Physiology 2009;297(1):H208-H222.

70.	Altes TA, Cloft HJ, Short JG, DeGast A, Do HM, *et al.* Creation of saccular aneurysms in the rabbit. American Journal of Roentgenology 2000;174(2):349-354.

71.	Kumar V, Abbas AK, Aster JC. Robbins basic pathology: Elsevier Health Sciences; 2012.